J. Fluid Mech. (1992), *vol.* 240, *pp.* 97–132
Printed in Great Britain

Lubricated pipelining: stability of core–annular flow. Part 5. Experiments and comparison with theory

By RUNYUAN BAI, KANGPING CHEN AND D. D. JOSEPH
Department of Aerospace Engineering and Mechanics, University of Minnesota, 107 Akerman Hall, 110 Union Street SE, Minneapolis, MN 55455, USA

(Received 20 April 1990 and in revised form 5 March 1991)

Results are given for experiments on water-lubricated pipelining of 6.01 P cylinder oil in a vertical apparatus in up- and downflow in regimes of modest flow rates, less than 3 ft/s. Measured values of the flow rates, holdup ratios, pressure gradients and flow types are presented and compared with theoretical predictions based on ideal laminar flow and on the predictions of the linear theory of stability. New flow types, not achieved in horizontal flows, are observed: bamboo waves in upflow and corkscrew waves in downflow. Nearly perfect core–annular flows are observed in downflows and these are nearly optimally efficient with values close to the ideal. The holdup ratio in upflow and fast downflow is a constant independent of the value and the ratio of values of the flow rates of oil and water. A vanishing holdup ratio can be achieved by fluidizing a long lubricated column of oil in the downflow of water. The results of experiments are compared with computations from ideal theory for perfect core–annular flow and from the linear theory of stability. Satisfactory agreements are achieved for the celerity and diagnosis of flow type. The wave is shown to be nearly stationary, convected with the oil core in this oil and all oils of relatively high viscosity. These results are robust with respect to moderate changes in the values of viscosity and surface tension. The computed wavelengths are somewhat smaller than the average length of the bamboo waves which are observed. This is explained by stretching effects of buoyancy and lubrication forces induced by the wave. Other points of agreement and disagreement are reviewed.

1. Introduction

Lubrication of oil by water in pipes appears to first have been mentioned in the patent application of Isaacs & Speed (1904). The density of the lubricating fluid here is greater than oil. They note that concentric flow may be established if a rotational motion is imparted to the flowing liquids by means of a rifle on the inside of the pipe. Their invention consists in making the fluid to be conveyed, together with a fluid of greater density, advance through the pipe with a helical motion, so that the denser fluid separates from the lighter and encases it, thus reducing the frictional resistance to the flow of the lighter fluid.

This idea may perhaps be usefully reformulated as a competition between centripetal and gravity forces, with film lubrication when centripetal acceleration is dominant, and vertically stratified flow when gravity is dominant (see for example Chernikin 1956). When gravity is dominant, stratified flow will result. Stratified flow can also be lubricated because part of the pipe wall is lubricated. Looman (1916)

patented a method of conveying oils or similar substances through pipes by passing them over relatively stationary bodies of water lying at the bottom of the pipe, i.e. an array of 'water traps' at the bottom of the horizontal pipe. (Obviously there would be no need for a water trap if the flow was already stratified.)

Theoretical methods are available for estimating pressure-drop reduction for completely stratified laminar flow. Yu & Sparrow (1967) and Charles & Redberger (1962) found that the ratio of the depth h of the lubricating layer to pipe radius R for maximum reduction is $h/R = 0.4$. The pressure-gradient reduction factor found by Yu & Sparrow is about 1.37 for liquids with a viscosity ratio greater than 1000; that found by Charles & Redberger (1962) was slightly smaller. Other theoretical studies which assume laminar flow and a flat interface are by Gemmell & Epstein (1962) and Ranger & Davis (1979). The experiments of Charles & Lilleleht (1966) and Kao & Park (1972) indicate that the 'perfectly stratified flow' assumed in these theoretical studies is stable for at least some of the operating conditions in their experiments. The discrepancies in the results of the experiments of Russell, Hodgson & Govier (1959) and Charles (1963) on nominally stratified flow of two immiscible liquids in circular pipes may be due to instabilities of perfectly stratified flow which have not yet been analysed. The same cause may be at the root of the difference between the idealized prediction for stratified laminar flow between infinitely wide parallel plates by Russell & Charles (1959) and experimental data for circular pipes.

The water in a stratified oil–water flow will tend to encapsulate the oil. This is a dynamic effect which is independent of the wetting properties between the liquids and the pipe walls. Charles & Lilleleht (1966) observed a curving of the interface in the neighbourhood of the duct walls, but concluded that this is not an effect of primary importance except in ducts of small horizontal dimensions. Bentwich (1976) has considered some problems of laminar stratified flow with an eccentric interface in the form of a circular arc. This could be called 'perfect partially stratified flow' and it would be unstable under certain conditions. It is not clear whether the Bentwich model captures some effects of encapsulation. We shall not consider vertically stratified flows further here, but they are important.

We have already noted that if the density difference between water and oil is not too great and if the viscosity difference is great enough, the water will automatically encapsulate the oil. The earliest application of this idea to the practice of pipelining that we could find is by Clark (1948, cited as a private communication by Russell & Charles 1959).

The patent application by Clark & Shapiro (1949), who did extensive tests in a three mile length of 6 in. pipe, is the first that appears to address the problem of core–annular flows of heavy petroleum. Here gravity effects are reduced by density matching to an acceptably small level and the heavy oil and water can flow in a lubricated manner, without stratification.

Clark & Shapiro emphasized the method of additives and surface-active agents in controlling the emulsification of water into oil. This is an undesirable condition since the emulsion has a higher viscosity than the oil alone, and when water emulsifies into oil, lubrication is lost. Emulsification occurs readily in the so-called 'light oils' with viscosities less than 500 cP. Lubricated pipelining is a viable proposition for heavy oils, which can be defined roughly as oils whose viscosity exceeds 500 cP with a density near to water, say $\rho_o > 0.9$ g cm^3.

An important series of experiments on water-lubricated pipelining, to be referred to below, were carried out in Alberta, Canada by Russell & Charles (1959), Russell *et al.* (1959), Charles (1963) and, especially, by Charles, Govier & Hodgson (1961,

hereafter referred to as CGH). Other experiments on water lubrication in pipes include those of Glass (1961) who found among other things that the lowest pressure gradients were achieved when the water input rate was between 30% and 40%, and Stein (1978) and Oliemans *et al.* (1985). Also Shell Oil has pioneered the development of commercially viable pipelines. Recently Maravan of PVSA (Petroleos de Venezuela Sociedad Autonomia) has placed in operation a 60 km line to transport heavy crudes in the lubricated mode. In general such lubricated lines become attractive when the lighter crudes are expensive or locally in short supply.

Finally we draw the reader's attention to some experiments which are indirectly related to water-lubricated pipelining. Shertok (1976) on flow development in a vertical pipe; Hasson, Man & Nir (1970) on film rupture in the pipe flow of water inside an annulus of slightly heavier and more viscous organic liquid; and Aul & Olbricht (1990) on the instability of an oil film of thickness $O(1\ \mu m)$ on the wall inside a capillary tube of 54 μm radius filled with water in an experiment is related to secondary oil recovery.

Oil, being lighter than water, will rise to the top of a horizontal pipe in which both are flowing together. The oil can then ride high in a pipe while being lubricated by a film of water all around, the film being thinner at the top than the bottom. Another possible arrangement occurs when the pressure gradients are not too small: the oil is again surrounded by a film of water but seizes parts of wall on the top where it runs as rivulets in the water. In some cases, there is oil at the top of pipe, with a film of water below it and the water completely lubricates an oil core. Ooms *et al.* (1984) developed a semi-empirical model to explain their experimental observation of a ripple core lubricated by water through a horizontal pipe. Data from experiments is required to make the model work. A later revision of this model by Oliemans *et al.* (1985) incorporates some effects of turbulence in the lubricating water.

Purely theoretical nonlinear amplitude equations for a plane layer based on lubrication theory have been given by Ooms *et al.* (1985), and by Frenkel *et al.* (1987), Frenkel (1988) and Papageorgiou, Maldarelli & Rumschitzki (1990). Chen & Joseph (1991) studied nonlinear problems which could be formulated as Ginzburg–Landau equations.

Since the effects of gravity destroy axisymmetry in horizontal pipes, the study of horizontal flow with gravity included is very difficult. None of the lubrication-based theories and none of the stability studies treat the asymmetric effects of gravity in horizontal pipes. This is a great misfortune since such effects are different and possibly more dangerous for lubrication in large than in small pipes, but scaling laws from mathematical analysis are unknown.

The effects of gravity are important even for the lubrication of heavy crudes. The oil and water will stratify whenever the flow is stopped. In general, the pressure gradients required for restarting a line which is filled with oil above and water below is much greater than for steady flow. Maximum load designs therefore are associated with startup. These maximum loads can, it turns out, be greatly reduced by the use of additives in the water. It is probable that large improvements in the technology of water lubrication can be achieved through manipulation of the material of pipe construction. The general goal would be to coat the inside of pipes with hydrophillic materials. We are unaware of systematic studies along these lines.

Perfect core–annular flow (PCAF) is an exact steady laminar solution of the problem of flow in a pipe of circular cross-section. PCAF is a rectilinear flow with one non-zero component of velocity that varies only with the radius coordinate. The two fluids are arranged centrally, one fluid in the core, the other in the annulus. This

solution possesses maximum symmetry. Since the effects of gravity are such as to destroy the axial symmetry in the problem for horizontal pipes, PCAF cannot be realized unless gravity is nullified by density matching as in the experiments of CGH. In vertical pipes of circular cross-section, the inclusion of gravity in the analysis does not break the axial symmetry present in the problem, and PCAF is possible without matching densities.

Analysis of the stability of PCAF shows that it is stable only for a very small set of conditions which typically do not occur in the applications. The other, more robust core flows, like wavy core flow, which are well-lubricated and well-liked in the oil industry are very different to PCAF so that it is not clear at the outset that stability studies will have a practical application. Fortunately it turns out that the study of the stability of PCAF is helpful in understanding, predicting and possibly in controlling the different flows which arise in the applications.

Hickox (1971) studied the linear theory of stability of PCAF in a vertical pipe with the long-wave approximation. All the principal physical effects – the viscosity ratio, the density ratio, the radius ratio of the interface to the pipe radius, surface tension, gravity and a Reynolds number – are in his governing equations. However, his analysis is restricted to long waves, up to first order in an expansion in powers of the wavenumber and only axisymmetric disturbances and disturbances with a first-mode azimuthal periodicity were considered. Hickox further restricted his study to the case in which the viscosity of the core is less than the annulus; water inside oil. He found all such flows are unstable to long waves. It is not clear why he did not consider the interesting case of lubricated pipelining in which the core viscosity is greater. This latter problem was studied by Joseph, Renardy & Renardy (1984*b*).

Ooms (1971) considered the stability of core–annular flow of two ideal liquids through a pipe. He found that the flow undergoes capillary instabilities and Kelvin–Helmholtz instabilities, due to a velocity difference at the interface. This difference is suppressed by viscosity and is replaced by a discontinuity in the velocity gradient. The flow is unstable to short waves if surface tension is zero in both the viscous and inviscid cases. The instability in the inviscid case is catastrophic, however; the growth rate goes to infinity with the wavenumber (Hadamard instability). The short-wave instability which arises in the viscous case when surface tension is zero was discovered by Hooper & Boyd (1983) and can be called a viscous regularization of the Kelvin–Helmholtz instability (see the review paper by Joseph & Saut 1990 for a discussion).

Preziosi, Chen & Joseph (1989, referred to hereafter as PCJ) extended the analysis of Joseph *et al.* (1984*b*) to include the effect of surface tension and density differences without gravity. They were the first to identify the lower branch of the neutral curve. Hu & Joseph (1989*a*) considered the three-layer problem with an oil film on the inside wall of the pipe and a lubricating layer of water between the oil film and oil core. They introduced the idea of forming an energy budget for the wave of maximum growth to identify the mechanisms of instability. Hu & Joseph (1989*b*) studied the stability of core–annular flow in a rotating pipe and Hu, Lundgren & Joseph (1990) studied the stability of core–annular flow for a highly viscous core.

Gravity is neglected in the foregoing studies, but was taken into account in the studies of core–annular flow in vertical pipes by Smith (1989) who neglected viscosity stratification and surface tension, and confined his study to long waves, and by Chen, Bai & Joseph (1990, referred to hereafter as CBJ) who included all effects and gave preliminary results of experiments reported fully here. Lin & Ibrahim (1990) studied a viscous liquid jet surrounded by a viscous gas in a vertical pipe in the presence of

gravity and interfacial tension. There is some overlap between their study and Hu & Joseph (1989*a*).

This paper reports the results of experiments on core–annular flow in a vertical pipe and correlates the observations with the results of computations using ideal theory and the linear theory of stability. The ∩ loop tube apparatus used in these experiments was described by CBJ but we will describe it in more detail in §2. The force of gravity is axial in this apparatus, in the direction of the pressure gradient in upflow and against the pressure gradient in downflow. We can account for all the principal physical effects in the stability study of these flows, i.e. the viscosity difference, the density difference, gravity, surface tension and the Reynolds number.

The flow charts presented in this paper are the first for vertical flow and surprising results for the holdup ratio and the pressure-gradient reduction are reported. The comparison of linear theory and experiments is the most extensive one so far reported and we find agreement between theory and experiments in certain specific regimes of flow.

2. Experimental set-up and procedures

The flow system is shown in figure 1. The density and viscosity of the water and oil used in our experiment at 22 °C are

$$(\rho_w, \mu_w) = (0.995 \text{ g cm}^3, 10^{-2} \text{ P}); \qquad (\rho_o, \mu_o) = (0.905 \text{ g cm}^3, 6.01 \text{ P}). \tag{2.1}$$

The pipeline is a ∩ loop which is mounted on the wall with its long legs vertical, aligned with gravity. The flow of oil and water to the pipeline is established by the pressure of compressed air in the oil and water tanks. The flow rates Q_o and Q_w of oil and water are controlled by valves at the outlets of the oil and water tanks. Q_w is measured by a rotameter and Q_o by a positive displacement gearmeter which is particularly suited to high-viscosity liquids. The oil and water are injected into the pipeline concentrically in an oil core and water annulus flow by means of a nozzle fitted centrally in the pipe. Water flows in the pipe and oil in the nozzle. Nozzles of different diameters were used: the 'best' diameter depending on flow conditions. The flow is first pushed up against gravity in the left leg of the loop, then turns around at the top of the loop and flows down in the right leg. There are test sections on the left and right legs which are enclosed in boxes filled with glycerine to remove lens distortion from the round walls of the pipe. The test section is 381 pipe diameters from the entrance at a height of 93 in. The total height of the loop is 180 in.

The loop system is closed, i.e. the oil and water are recirculated, being stored in separate pressurized tanks. The pressure levels in the two tanks are adjustable and drive the liquids to the loop without pulses. The oil and water are ejected into a large tank and separated under gravity. After separation the two liquids are driven back into the inlet storage tanks by compressed air.

Pressure drops are measured in the up- and downflow legs of the loop. In each leg there are two pressure taps connected to a manometer. The pressure taps are designed to facilitate the separation of oil from the water so that only water will enter the manometer. The pressure gradient cannot simply read off the manometer when there are two fluids in the pipe, and we found that

$$\Delta p = \rho_w g\hat{H} + (\rho_w - \rho_o) g H_o \tag{2.2}$$

is the pressure drop due to motion in upflow, where $\hat{H}$ is the height of water in the manometer tube, H_o the height of the oil head and g the acceleration due to gravity.

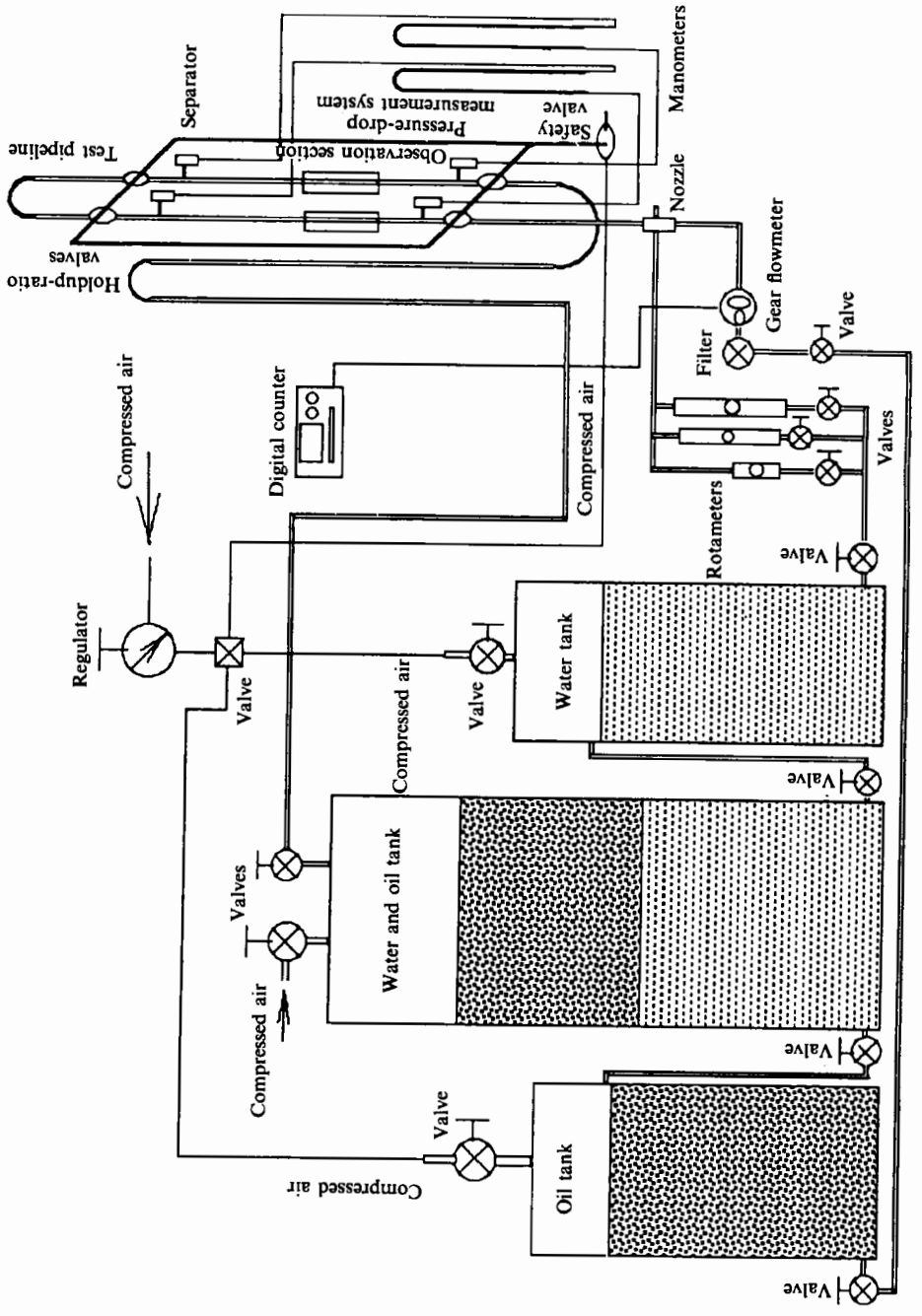

FIGURE 1. The experimental system.

In downflow where the pressure gradient and relative buoyancy are opposed, the height difference of the manometer legs is proportional to Δp *plus* the hydrostatic contribution so that

$$\Delta p = \rho_w g\hat{H} - (\rho_w - \rho_o) g H_0. \tag{2.3}$$

We may have flow, due to relative buoyancy alone, for which $\hat{H} = 0$.

Formulae (2.2) and (2.3) require measured values of $\hat{H}$ and H_0. The height difference $\hat{H}$ is read directly in the manometer but H_0 depends on the volume of oil between the pressure taps in the pipe and it cannot be determined directly. To determine H_0, we measure the volumes of oil and water between the pressure taps directly by means of two valves, called holdup valves, which cut off the flow between the taps simultaneously. There is a third safety valve which opens at the same time that the holdup valves are closed, releasing the high pressure in the system. After the holdup valves are closed, the oil rises and the volumes of oil and water are read easily. The distances between the holdup valves and pressure taps are 93 and 90 in. respectively so that the measured heights must be reduced by 90/93. Since the diameter ($d = \frac{3}{8}$ in.) of all pipes is the same, we may easily compute volumes by measuring heights. There are two sets of holdup valves, one for upflow and one for downflow.

All the data taken in our experiments are recorded on our Kodak Spin Physics 2000 Motion Analysis System or on a high-resolution video camera. The only quantities that can be controlled after an experiment is set-up are the flow rates of oil and water. We fix one of the flow rates and vary the other. Then we wait for transients to decay. The slower flow rates have long transients. After steady conditions are established, video recordings are made. The high-speed recordings contain the raw data for the analyses of the flow: the recording can be seen in slow motion; or stopped; or step advanced. This allows us to measure the distances, say, between crests of waves and their phase speed (celerity). The size and speed of slugs and bubbles and the correlation of flow types with operating conditions can all be determined from these video recordings. For this paper we were interested in flow type and average wavelengths and wave speeds. These are simple averages obtained by summing values and dividing by the number of trials. Our stored data can also be analysed for the spectral properties of the waves, which should be useful for projected studies of the nonlinear properties of wavy flow.

To correlate the experimental observations with the linear theory of stability, we need to specify whether the flow is up or down, the two flow rates and the water fraction in the pipe. The water fraction is a functional of the solution determined by the holdup ratio in the manner described below.

3. Holdup ratio in upflow and downflow

Conventional wisdom about holdup ratios in lubricated pipelining needs to be amended to include effects of buoyancy in vertical pipes. The holdup ratio (3.1) is a ratio of ratios: the ratio of volume flow rates to the ratio of volumes. These two ratios would be the same, i.e. $h = 1$, in a perfectly mixed flow, say a well-emulsified solution of water in oil. In general, and certainly in lubricated pipelining, the two fluids are not well-mixed and the holdup ratio differs from unity. It is generally thought that the liquid in contact with the pipe wall tends to be held back. Thus the holdup will tend to be greater than unity when the water is the component in contact with the pipe wall and to be less than unity when oil is in contact with the pipe wall. This is not correct in vertical flow where the effects of buoyancy are important.

Because the up- and downflow legs of our loop apparatus are connected, the pressure drop is established over the whole pipe with a continuous loss of pressure due to friction. The reader may be helped by thinking that to a first approximation the pressure gradient is a constant, the same constant in the up and down legs of the loop apparatus. Gravity aids the applied pressure gradient in accelerating the oil relative to water in the upflow and decelerating the oil relative to the water in the downflow. This means that more oil accumulates in downflow than in upflow. The water fraction is greater in upflow than in downflow:

$$h = \frac{Q_o/Q_w}{\Omega_o/\Omega_w} = \frac{V_o/V_w}{H_o/H_w} = \frac{V_o/V_w}{A_o/A_w}, \tag{3.1}$$

where Ω_o and Ω_w are the volumes of oil and water respectively, V_o and V_w are their respective superficial velocities, $A_o = \pi R_1^2$, $A_w = \pi(R_2^2 - R_1^2)$ and R_1 and R_2 are respectively the mean radius of the oil/water interface and the inside radius of the pipe. Also, $A_w/A_o = a^2 - 1$ and $a = R_2/R_1$. After replacing Ω_o/Ω_w with $a^2 - 1$ in (3.1), we obtain

$$a = (1 + hQ_w/Q_o)^{\frac{1}{2}} = (1 + hV_w/V_o)^{\frac{1}{2}}. \tag{3.2}$$

This formula is particularly important because experiments show that h is constant in upflow and fast flow.

The value $h = 0$ of the holdup ratio can never be achieved in upflow or horizontal flow, but it can be realized in downflow, when there is already oil in the pipe, $\Omega_o \neq 0$, but no new oil supply is forthcoming, $Q_o = 0$. An experimental realization of this in downflow is shown in figure 2 where a long oil slug with aspect ratio in excess of 20 is exhibited. This slug is perfectly lubricated by water. Basically we can say that the slug is fluidized, it is lifted by gravity against the oncoming downflow of water, suspended in the lubricating stream in an equilibrium of weight and drag. It is possible to suspend truly large slugs with aspect ratios greater than 100 in this way.

In figure 3 we have plotted the volume ratio $\Omega_o/\Omega = H_o/L$ ($L = H_o + H_w$), where $\Omega = \Omega_o + \Omega_w = \pi R_2^2(H_o + H_w)$ is the total volume, against the input flow ratio $Q_o/Q_w = V_o/V_w$. We can fit the data for upflow closely to the empirical curve

$$H_o/L = 1 - 1/(1 + 0.72V_o/V_w). \tag{3.3}$$

Hence $H_w/L = 1/(1 + 0.72V_o/V_w)$ and

$$h = \frac{Q_o}{Q_w}\frac{\Omega_w}{\Omega_o} = \frac{V_o}{V_w}\frac{H_w}{H_o} = \frac{1}{0.72}. \tag{3.4}$$

This shows that h is constant in upflow of cylinder oil in water and is independent of any input ratio or flow condition.

Figure 4 is for downflow. The data points are more scattered in down- than in upflow, especially for moderate input ratios. The empirical formula (3.3) which works for upflow does not work as well in downflow. The difference between upflow and downflow is more clearly expressed in figure 5.

One major conclusion implied by the data shown in figures 3 and 5 is that the holdup ratio h in upflow does not depend on the flow rates of oil and water or on the ratio of flow rates. The holdup ratio in downflow depends strongly on these parameters, as is shown in figures 4 and 5. These figures show that when the flow rates are large the effects of gravity are suppressed, as are the differences between up- and downflow. Hence in fast flows the holdup ratios are the same and equal to approximately 1.39 in both up- and downflow. This result agrees with conventional

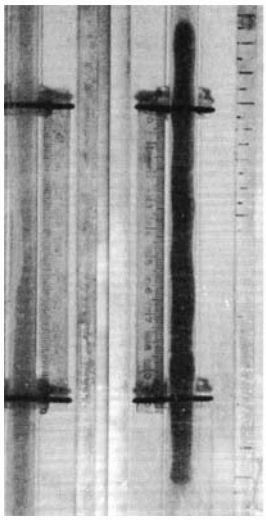

FIGURE 2. Long oil slug suspended by gravity in downflow of water when the water flow rate is about 0.04 ft/s. The slug is fluidized, in equilibrium under weight and drag. The holdup ratio is zero. Transient travelling spiral waves, called corkscrews, can be seen on different segments of the core. It is easy to fluidize much longer slugs, even to have a continous core of oil fill the entire downflow pipe.

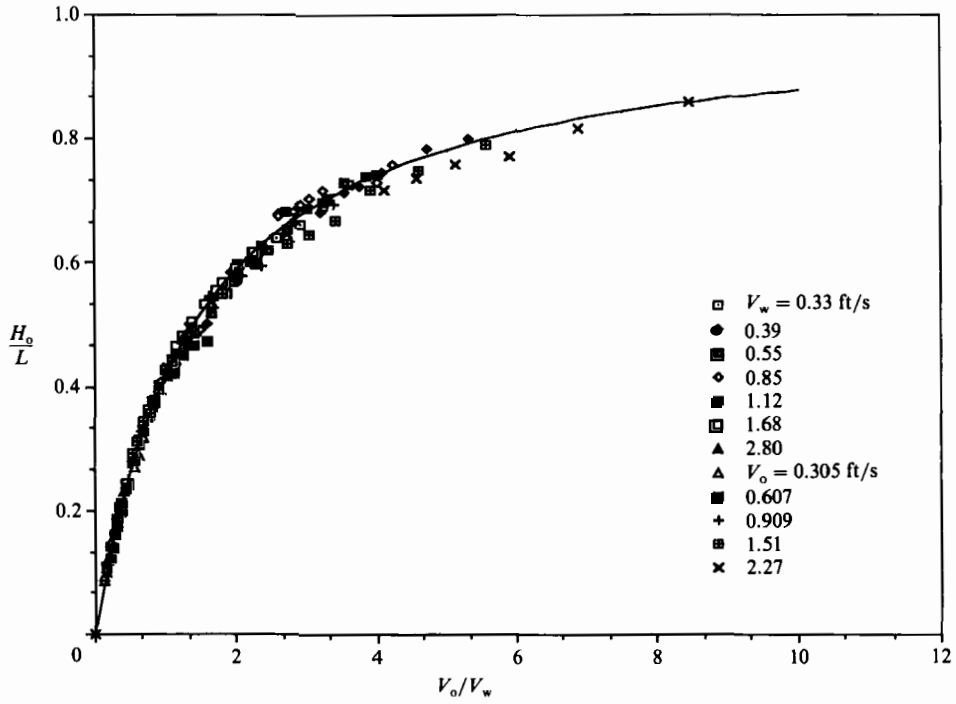

FIGURE 3. The volume ratio $\Omega_o/\Omega = H_o/L$ versus the input ratio V_o/V_w for upflow. The data fall close to the solid line given by (3.3).

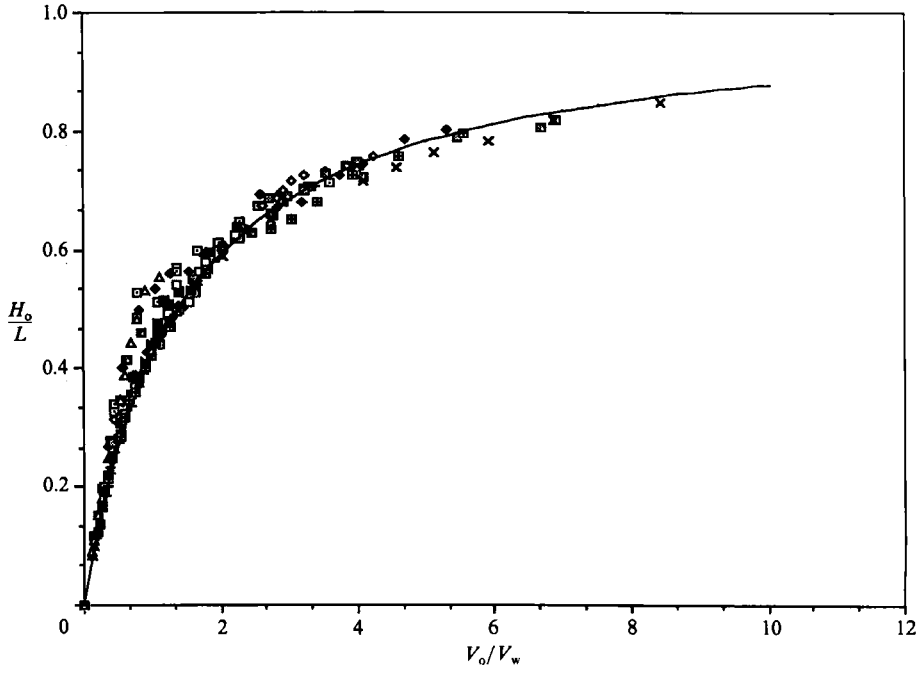

FIGURE 4. The volume ratio versus input ratio for downflow. The formula (3.3) is plotted. The data points are as in figure 3.

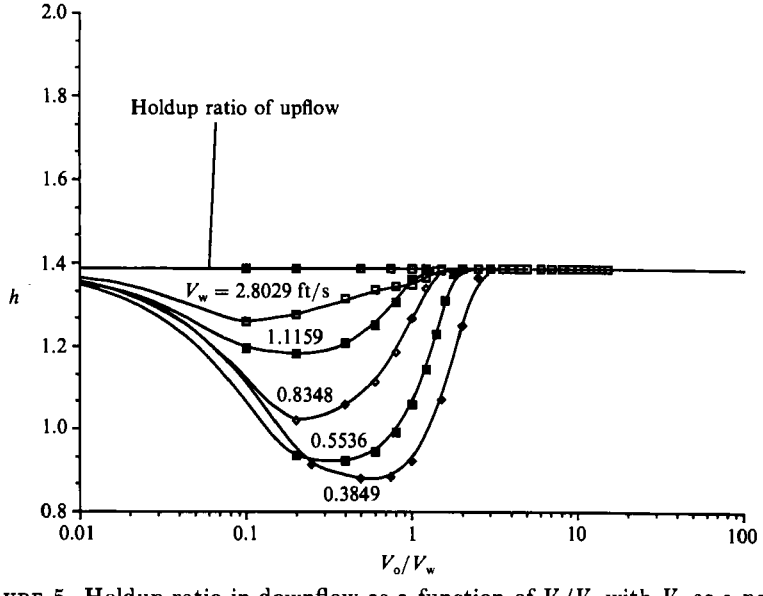

FIGURE 5. Holdup ratio in downflow as a function of V_o/V_w with V_w as a parameter.

wisdom, i.e. the water is being held up, but disagrees with results of CGH who found that in horizontal pipes, when the densities of oil and water are matched, the holdup ratio does depend on the input ratio and flow velocity, even at large flow rates.

4. Flow types

About six or seven qualitatively different flow regimes can be distinguished in experiments. There is some subjectivity involved in the delineation of differences so that the exact number of qualitatively different regimes may differ slightly from observer to observer. The flow regimes which appear in horizontal pipes under conditions of matched density have been already identified in the paper by CGH who studied concurrent flow of water and oil–carbon tetrachloride solution in a 1.04 in diameter pipe. Some of the different regimes observed by them were studied theoretically by Hu & Joseph (1989*a*, *b*) PCJ, and CBJ. Many of the regimes of flow identified by CGH and some new ones, for example, bamboo waves, appear in vertical flow. We were not able to study the important regime in which water emulsifies into the oil, called 'water droplets' by CGH, because our apparatus is not strong enough to withstand the high pressure gradients generated in this condition in which water lubrication fails.

In this section we shall give a qualitative description of the types of flow we encountered, together with illustrative photographs and a discussion of some underlying physical mechanisms associated with the different flow types. Different types of flow are associated with different regions on a flow chart whose coordinates may be chosen as the superficial velocities of oil and water. The disposition of the flow types on the flow chart is considered in §5.

4.1. *Oil bubbles in water*

These bubbles arise from capillary instabilities in the presence of shear. Oil bubbles in water are produced by capillarity but the size of the bubbles is determined by other factors, like shear, as well. The range of sizes of the bubbles which are observed is fairly well predicted by the linear theory of stability using Rayleigh's idea that the size of the bubble which will be observed corresponds to one-half of the length of maximum growth. Of course, in the present case, shear flow has a strong influence on the length of maximum growth. PCJ investigated this idea by comparing calculations from the linear theory of stability with the size of bubbles observed in the experiments of CGH. Their results, reported in their table 1, show good agreement.

As a rule of thumb, we can say that we will always have oil bubbles in water if there is a large amount of water. Dispersions of oil in water, rather than bubbles, appear when the water velocity is much larger than the oil velocity. Dispersions will be discussed in §4.7 below.

There is a marked difference in the distribution of bubbles in upflow and in downflow, even when they are of approximately the same size. In upflow the bubbles tend to spread and distribute themselves uniformly in the pipe. The wake interactions are weak because the velocity of the oil relative to the water is small. The oil is lifted by gravity relative to a forced stream of water moving in the same direction. Bubbles in downflow tend to aggregate. Wake forces between bubbles in downflow are much greater than in upflow because the bubbles are lifted against the forced stream of water, producing larger relative velocities and stronger wakes.

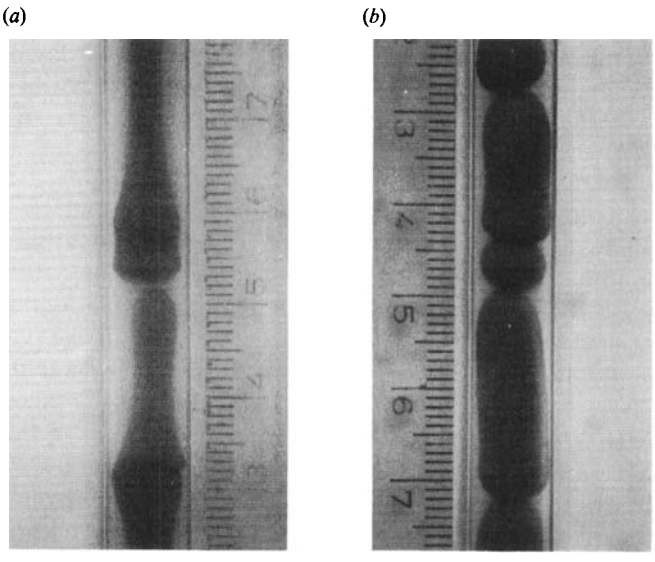

FIGURE 6. Oil slugs in water. (*a*) Upflow. The larger bubbles are stretched out under the action of shear and buoyancy. This is shear stabilization of slugs and bubbles leading to long bamboo waves. (*b*) Downflow. The oil is held by buoyancy and slugs held together by wakes forming long trains.

4.2. *Slugs of oil in water*

If an oil bubble in water has a natural diameter larger than the pipe diameter, one way to get the entire volume into the pipe is to squash the bubble into a capsule shape. These capsule shapes are dynamically possible because they are shear stabilized by water. They move through the pipe freely lubricated on all sides by water in a manner reminiscent of capsule transport in pneumatic tubes.

Slugs form readily from bubble aggregates in downflow when the oil fraction is increased. The bubble aggregates collapse to form longer slugs which have a relatively large diameter lubricated by a thin layer of water. Long slugs are like segments of PCAF, but they support corkscrew waves. Corkscrew waves look like a periodically buckled wimpy rod which rotates in the water due to hydrodynamic torques. Corkscrew waves on a long shear stabilized slug are shown in figure 2.

It seems to be impossible to create capsule slugs and corkscrew waves in upflow, where bubbles do not aggregate to form slugs as the oil input is increased. Instead filaments are pulled out, the bubbles are stretched, as shown in the photograph of figure 6, under the combined action of buoyancy and lubrication forces described in the caption of figure 8. This filamentation gives rise to the bamboo waves which are described next.

4.3. *Bamboo waves*

The shear stabilization of capillary instabilities in upflow leads to a regime of wavy flow in trains of sharp crests connected by long filaments. We call these bamboo waves. Superficially they resemble Stokes waves except that they perturb a cylinder and are imperfect. The filaments which connect the crests thicken as the oil velocity V_0 is increased for a fixed V_w and the average length of a wave decreases. These effects are evident in the photographs exhibited in figure 7. These waves are nearly stationary in a coordinate system moving with the undisturbed interface velocity so that the wave speed relative to laboratory coordinates also increases with increasing oil input.

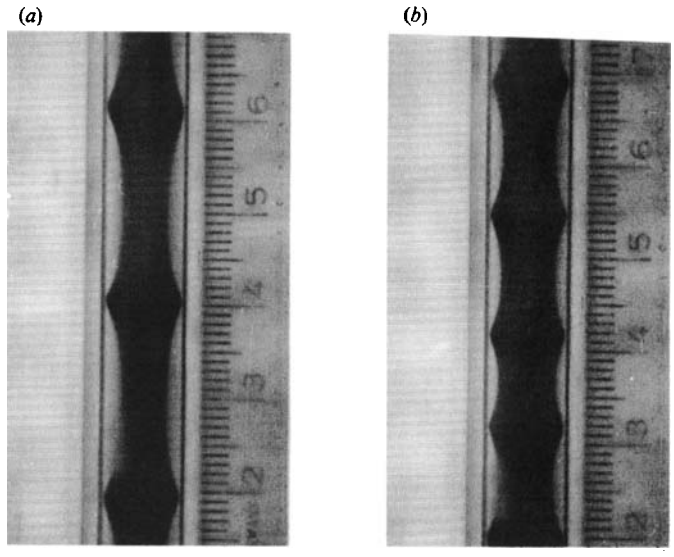

FIGURE 7. (*a*) Thin and (*b*) thick bamboo waves. The bamboo thickens and the average length of a wave decreases when the oil velocity increases at a fixed value of the water velocity. Some very short bamboo waves associated with high input velocities are shown in figure 9.

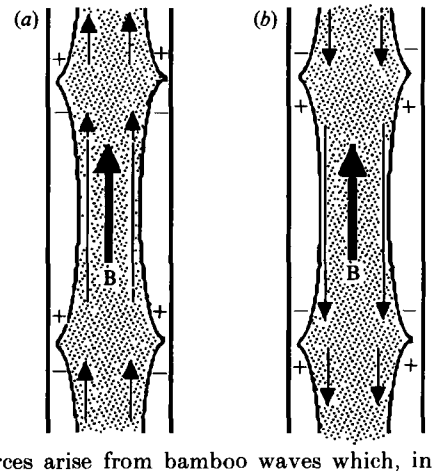

FIGURE 8. Lubrication forces arise from bamboo waves which, in the first approximation, are connected with the oil relative to stationary walls. The pressures which develop in the water in the front and back of crests are designated by + and − respectively and buoyancy of oil relative to water is designated by B. The pressure forces and buoyancy work together in upflow (*a*) where they lead to stretching and are opposed in downflow (*b*) where they lead compression and buckling.

Bamboo waves are a very robust regime of upflow, occupying a large area in the upflow charts shown in figures 13–16. They seem to maintain well-defined average wavelengths and wave speeds, but they are imperfect. The overtaking of one crest by another and the transient stretching of filaments between the waves is a frequent occurrence.

Bamboo waves in upflow are stretched owing to the combined action of buoyancy and lubrication forces. The buoyancy part of this mechanism is simply that the oil is lifted by gravity relative to the heavy water which in any event is stationary on the pipe wall. The crest of a wave on the oil must move forward relative to the water.

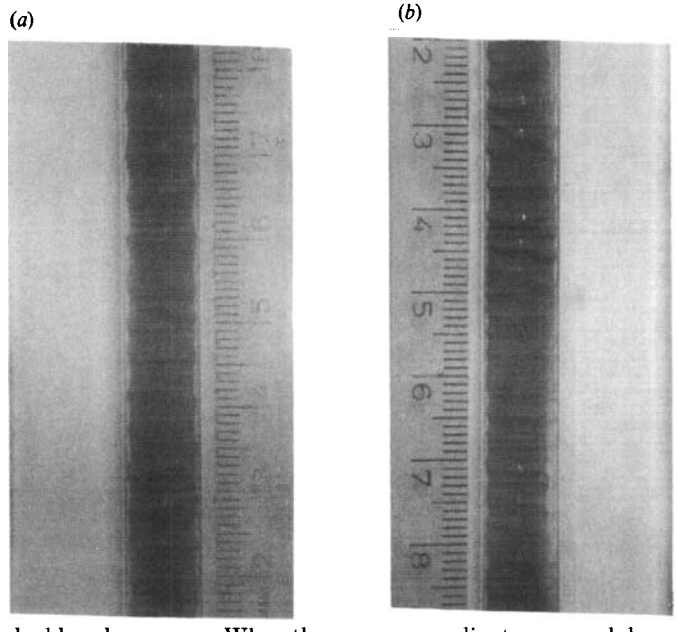

FIGURE 9. Disturbed bamboo waves. When the pressure gradients are much larger than buoyancy, the difference between upflow (*a*) and downflow (*b*) is suppressed. One sees short, thick-stemmed waves. The effects of stretching in upflow and compression in downflow are still active in producing longer waves in upflow.

We have already noted that the wave is nearly stationary, convected with the oil, unable to move fast on the oil core because the oil is so viscous. This means that there will be a positive buildup of pressure on the up side and a decrease of pressure on the down side of every crest in upflow, as shown in figure 8. The pressure associated with this lubrication effect will induce stretching in the same sense as buoyancy, elongating the wave, stretching the stems. On the other hand, the effects of buoyancy and lubrication are opposed in downflow. This tends to compress, even to eliminate, bamboo waves and may lead to the form of buckling which we have called corkscrew.

4.4. *Disturbed bamboo waves*

We have already mentioned that when the driving pressure gradients are relatively large and the flow is fast, the differences between up- and downflow vanish. In particular, the asymmetric effects of buoyancy on the holdup ratio are relatively less important when the pressure gradients are large. This can be seen in the disturbed up- and downflow bamboo waves shown in figure 9. Some effects of buoyancy on the wavelengths are still in evidence, with waves stretched in upflow and compressed in downflow. At a lower speed, the upflow waves elongate and the bamboo stems thin, while in downflow the stems thicken into columns of oil which support perfect core–annular flow which is perturbed by corkscrew waves from place to place. At a faster speed the oil core cannot keep its integrity and various kinds of dispersions of oil in water and water in oil will form.

4.5. *Disturbed core–annular flow (DCAF) and corkscrew waves*

Perfect core–annular flow (PCAF) is the basic flow whose stability was studied in the references mentioned in the introduction. In PCAF the core has a perfectly cylindrical interface of uniform radius which is perfectly centred on the pipe axis

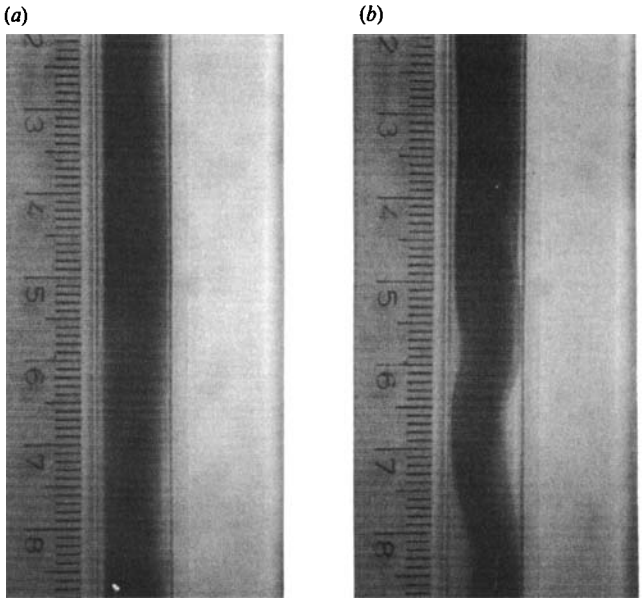

FIGURE 10. Disturbed core annular flow (DCAF). Some portions of the oil column in downflow are nearly perfect (*a*) while others are buckled and rotate as a corkscrew (*b*).

with an annulus of lubricating water outside. Good photographs of PCAF are shown in figures of CBJ. Figure 10 of this paper shows PCAF disturbed by transient spiral waves which we call corkscrew. We call this regime of flow disturbed core–annular flow (DCAF). Actually, the motion of a corkscrew as it is screwed down into the cork is an accurate description of the waves we see. These waves are not understood by us but they can perhaps be likened to the buckling of a very soft rubber when loaded with shear traction, which in our experiments is generated by the motion of water in the annulus. The apparent velocity of advance of the turning corkscrew is larger than the superficial velocity of oil or water. When the water flow rate is fixed in the small to moderate range where corkscrew waves appear, the pitch of the screw will increase with increasing rates of flow of oil leading to an apparent slowing of the wave. In this way one can obtain nearly perfect core–annular flow.

4.6. *Oil sticks to the wall*

The glass wall of the pipe is wetted preferentially by water. However, when the water flow rate is small and that of oil large, oil can displace the water on the wall of the pipe. This usually happens first in upflow. At still higher values of the oil flow rate, water will disperse or emulsify into oil. This dispersion is discussed in §4.7 below.

The deposition of oil on the pipe wall can sometimes be observed as a slow propagation of the wetting front with oil on the wall behind the front and water on the wall before the front. We call this phenomenon 'chugging'. Two chugging configurations in upflow are exhibited in figure 11. To achieve chugging we increase the oil flow rate, keeping the water rate constant. In figures 11(*a*) and 11(*b*) an oil core plus oil bubbles are ejected from the sheath of oil on the wall. Evidently there is an annulus of water between the sheath and the core. There is a blockage when the oil seizes the wall which is relieved by a three-layer configuration of oil core–water annulus–oil sheath. Shearing forces tear away many oil bubbles which form a cloud

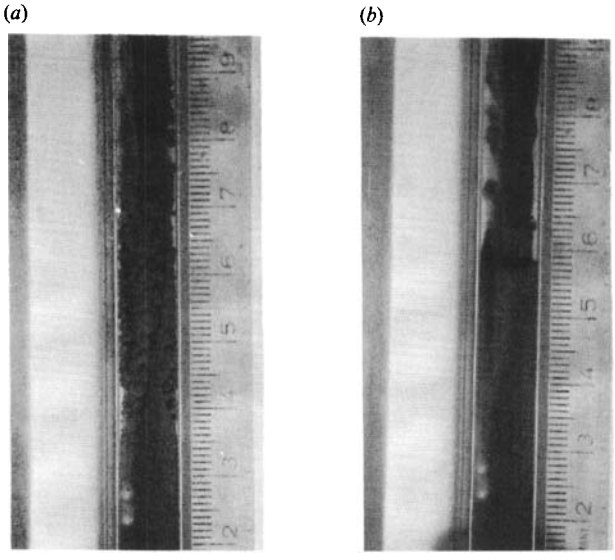

FIGURE 11. Deposition of oil on the wall. Oil seizes the hydrophillic glass wall when the oil flow rate is increased at a small fixed water flow rate (see 'oil sticks to the wall' on the flow charts in §5). After the oil seizes the wall, the pipe is blocked and the blockage is relieved by an oil core–water annulus–oil sheath configuration. (*a*) A bubble cloud around an internal core. (*b*) A clearer picture of the ejected core.

around an oil core in figure 11 (*a*), more clearly seen in figure 11 (*b*). If the oil flow rate is increased further, more oil bubbles than in figure 11 (*a*) will be formed followed by a phase inversion in which water droplets emulsify and oil becomes the continuous phase. This leads to a loss of lubrication and to huge increases in the pressure gradient.

The fact that oil replaces water on a hydrophillic wall under certain repeatable dynamical conditions is of wide interest because the complete solution of the problem of wetting and spreading cannot be solved by thermodynamic and generalized energy considerations; it is not only a problem of finding good constitutive models. The answer to the question 'When two fluids flow, which one will be on the wall?' depends on the history of the motion as well as the properties and interactions of the two fluids and the wall.

In figure 12 we see that oil may be deposited or removed from the hydrophillic glass pipe. Joseph, Singh & Chen (1990) showed how oil could be absorbed on the Plexiglas wall of a Taylor apparatus at the downflow cell boundary of a Taylor cell of an emulsified oil, but not elsewhere. This 'painted' configuration of absorption remains 'forever', even after the motion is put to rest. People who actually work for a living know they have to wash their hands to get them clean.

CGH found water lubrication for three different oils, 6.29, 16.8 and 65.0 cP, in a 1.04 in. cellulose acetate–butyrate pipe which is *hydrophobic*. This shows that water lubrication is mainly a dynamical effect, with a secondary role played by wettability. To more fully understand this we need to consider the problem of *phase inversion* which is considered in the next subsection. Hasson *et al.* (1970) studied core flow of water in a heavier 1.02 g cm^3 organic liquid (kerosene–perchlorthylene solution). They did not know that their flow was unstable because the organic solution has a higher viscosity.

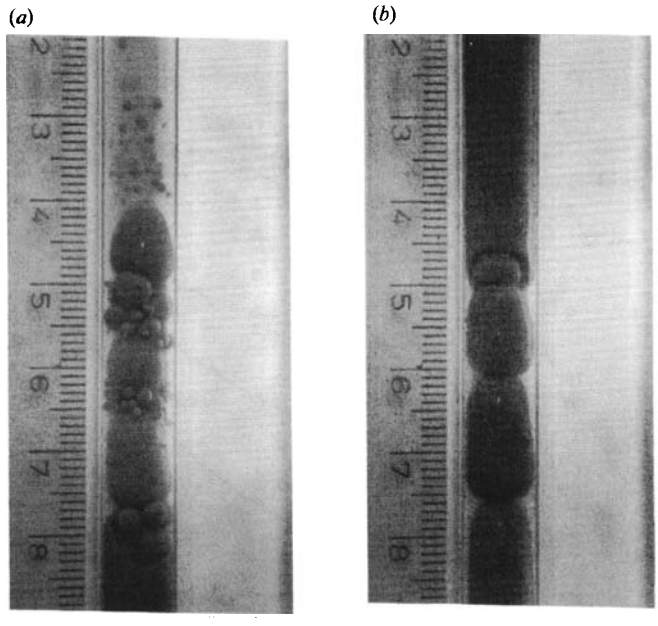

FIGURE 12. (*a*) Removal of oil from the hydrophillic wall in downflow. Look at the bottom of the photograph. Oil is being removed from the wall. Slugs and bubbles are entering the oil sheath where they are lubricated by water. (*b*) Oil is deposited on the wall in downflow. Slugs and bubbles are ejected from the sheath.

4.7. *Dispersions; phase inversion*

There is evidently a dispersion limit in which large bubbles, slugs, sheets, and other coherent bodies of a single fluid are broken up by forces associated with the motion. A dispersion of immiscible liquids, one of which is polar, the other non-polar, is often called an oil and water dispersion or emulsion. An emulsion is a stable dispersion, but stability here is defined in a time frame so that a dispersion over a long time can be considered an emulsion over a short time. There are water in oil (w/o) dispersions and oil in water dispersions (o/w), and under certain conditions one will change to the other. This is called a phase inversion. It is also possible for o/w and w/o dispersions to coexist. The formation of dispersions, their natural properties and phase inversion have been studied in different systems: CGH give some data for dispersions in core–annular flow of oil and water. Joseph *et al.* (1990) have studied dispersions of oil and water and dispersions of silicone and vegetable oil in a Taylor–Couette apparatus.

Dispersions will always form in two immiscible liquids where their motion is sufficiently intense. CGH gave data for the formation of dispersions; w/o dispersions were called 'water drops in oil' and o/w dispersions were called 'oil drops in water'. Generally a drop is heavier than the host fluid and in this sense the phrase 'oil drops in water' is a misnomer.

This distinction between small bubbles of oil in water and o/w dispersions can be fuzzy. PCJ calculated the size of a small bubble which arose in the experiment of CGH on 'oil drops in water'. The computed size was $\frac{4}{3}$ the size of the largest oil bubble in the dispersion. The other bubbles in the dispersion were much smaller. Perhaps the study of the size of single drops and bubbles in different flows is fundamental in distinguishing between bubbles and dispersions.

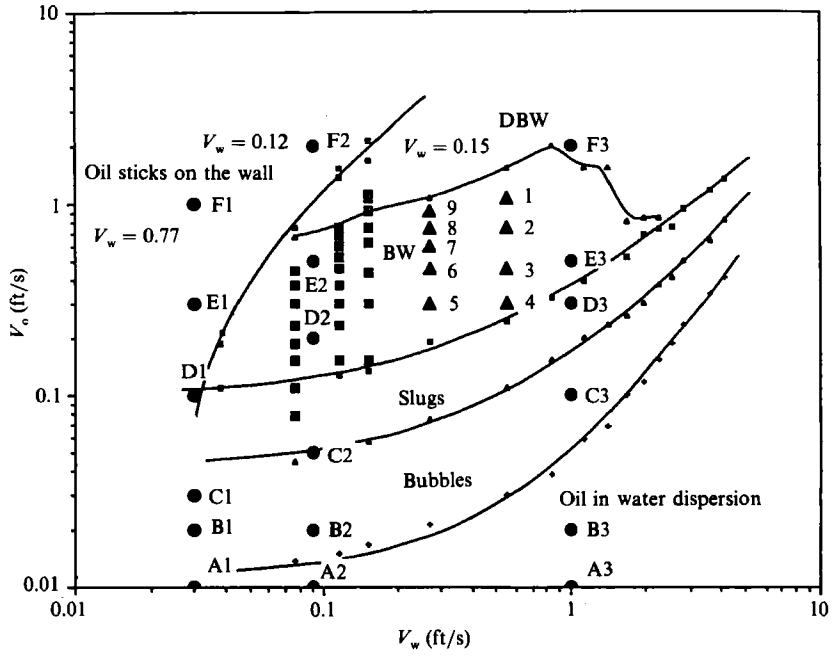

FIGURE 13. Flow condition in upflow as a function of the superficial water (with sodium silicate) velocity $V_w = Q_w/A$ and oil velocity $V_o = Q_o/A$. The holdup ratio is universally $h = 1.39$ (see figure 5) and the value of $a = R_2/R_1$ can be obtained from (3.2) for each and every point. The labelled circles and triangles are calculated and identified for comparison with theory in §8. BW denotes bamboo waves and DBW disturbed bamboo waves.

The o/w dispersions are a lubricated regime of flow, which is of interest since they burn with reduced NO_x and particulate emissions.

We could not emulsify water into oil with our apparatus. Water in oil dispersions has a higher viscosity than oil alone; lubrication is lost and the resulting pressure gradients are greater than the apparatus could withstand. The w/o dispersions have higher oil flow rates than that when oil seizes the wall. If we tried to increase the flow of oil, the pressure gradient would shoot up. If we could run the apparatus at the high pressure, a phase inversion to a w/o dispersion would probably result. The w/o dispersions and phase inversion from o/w dispersions are dangerous because they destroy lubrication.

5. Flow charts

A flow chart is a graph in the (V_w, V_o)-plane in which regions of different flow types are designated. The holdup ratio h for each (V_w, V_o)-point may be obtained from figure 5 and the corresponding value of the water fraction is given by $a = R_2/R_1$ from (3.4). The determination of a for a given (V_w, V_o) is simplified by the fact that $h = 1.38$ universally in upflow and for fast downflows.

In figure 13 we have plotted a chart showing the flow type of an emulsified oil of viscosity near 5 P in upflow of 0.4% aqueous sodium silicate solution. The flow condition is identified by points in the (V_w, V_o)-plane, where $V_w = Q_w/A$ is the superficial velocity of the water and V_o is the superficial velocity of the oil; and $A = \pi R_2^2$.

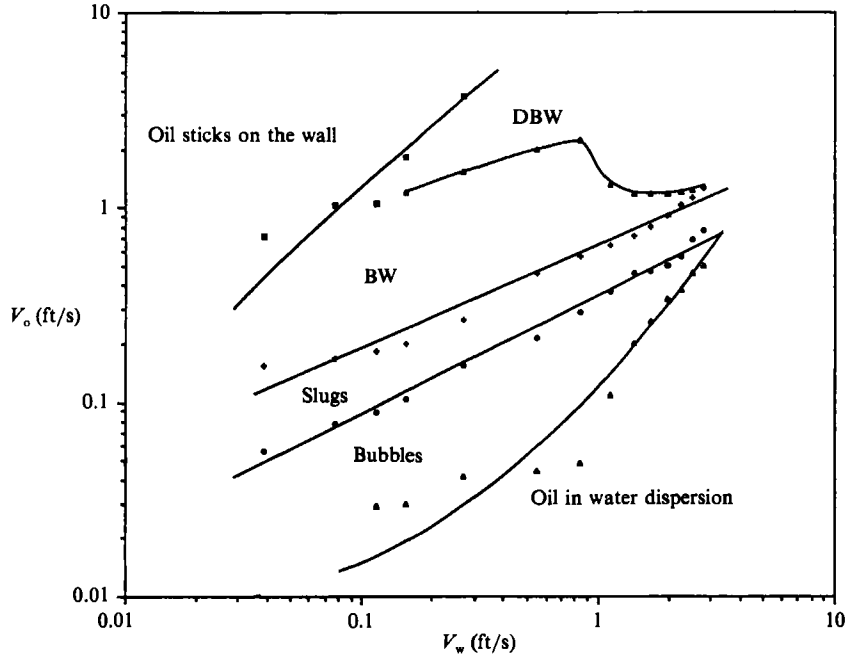

FIGURE 14. Flow chart in upflow as in figure 13 except that fresh water is used in a freshly cleaned pipe. There is a small upward shift probably due to a decrease in the water fraction, $h = 1.39$ for this flow.

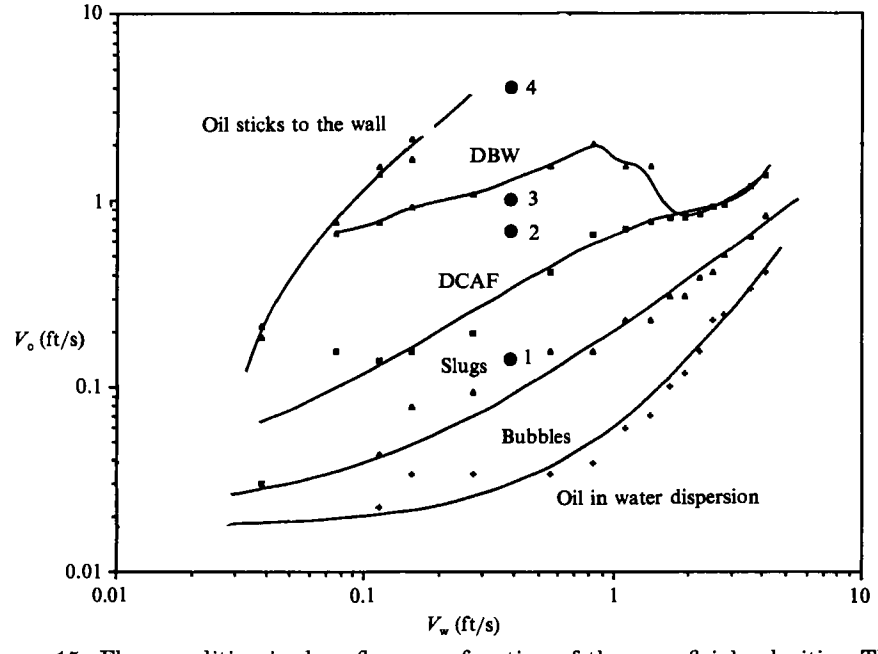

FIGURE 15. Flow condition in downflow as a function of the superficial velocities. The value of $a = R_2/R_1$ can be determined from (3.2) when the holdup ratio h is given by experiment as in figure 5. Disturbance in DCAF are corkscrew waves near the slug boundary and immature bamboo waves near the DBW boundary. The four circles are computed points. The linear theory of stability is discussed in §8.

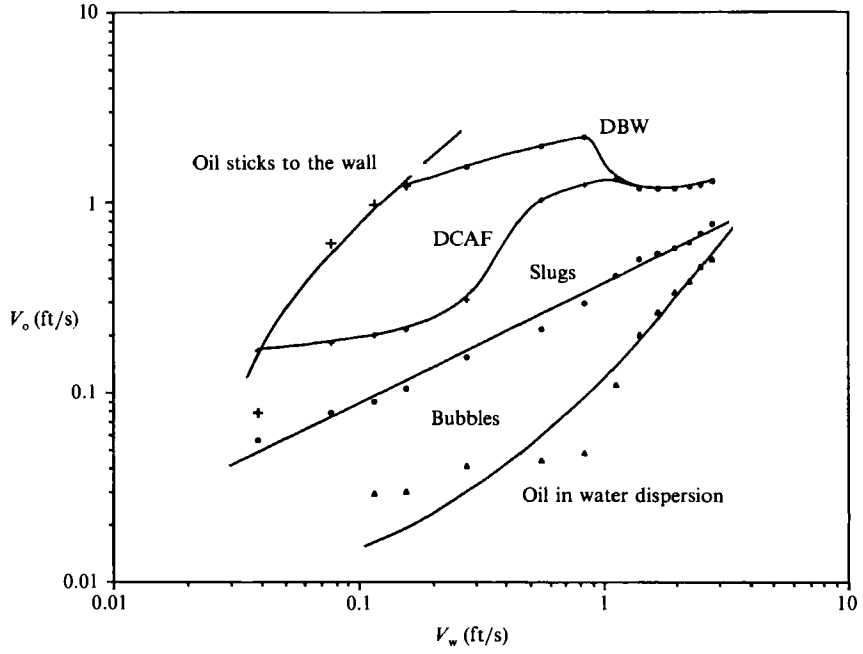

FIGURE 16. Flow chart for downflow as in figure 15 except that fresh water is used in a newly cleaned pipe.

In figure 14 we plotted a flow chart for upflow using the same oil with pure water in a freshly cleaned pipe. Figure 15 is a flow chart for downflow under the condition specified in figure 13. Figure 16 is the downflow chart using fresh water in a freshly cleaned pipe.

The figures may be compared with the flow charts of CGH. The flow types are not the same; they did not have bamboo waves or disturbed core–annular flow with corkscrew waves and we could not achieve the pressure gradients necessary for emulsification of water into oil. Nevertheless, the interested reader will find the way to identify similar regimes. The regularity with which flow types fall on flow charts is gratifying.

6. Pressure-drop measurements

Data on pressure drops and holdup ratios were obtained for different flow rates of oil and water. We express the flow rates Q_w, Q_o in terms of superficial velocities $(V_w, V_o) = (Q_w, Q_o)/A$ in ft/s where $A = \frac{1}{4}\pi d^2$ and $d = 2R_2 = \frac{3}{8}$ in. Data were taken for seven values of V_w: 0.329, 0.385, 0.554, 0.834, 1.116, 1.678, 2.803 and five values of V_o: 0.305, 0.607, 0.909, 1.513 and 2.269. We fix V_w (or V_o) and take measurements for all V_o (or V_w). We measure Δp by manometer measurements using (2.2) and (2.3). The pressure gradient due to motion is $\Delta p/L$. We define a dimensionless pressure gradient

$$\Theta = \Delta p/\rho_w g L, \tag{6.1}$$

which is expressed as feet of water/foot. Measured values of the pressure drop *vs.* the flow rate ratio with V_w as a parameter are given in figure 17.

Measured values of the pressure drop *vs.* the flow rate ratio with V_o as a parameter

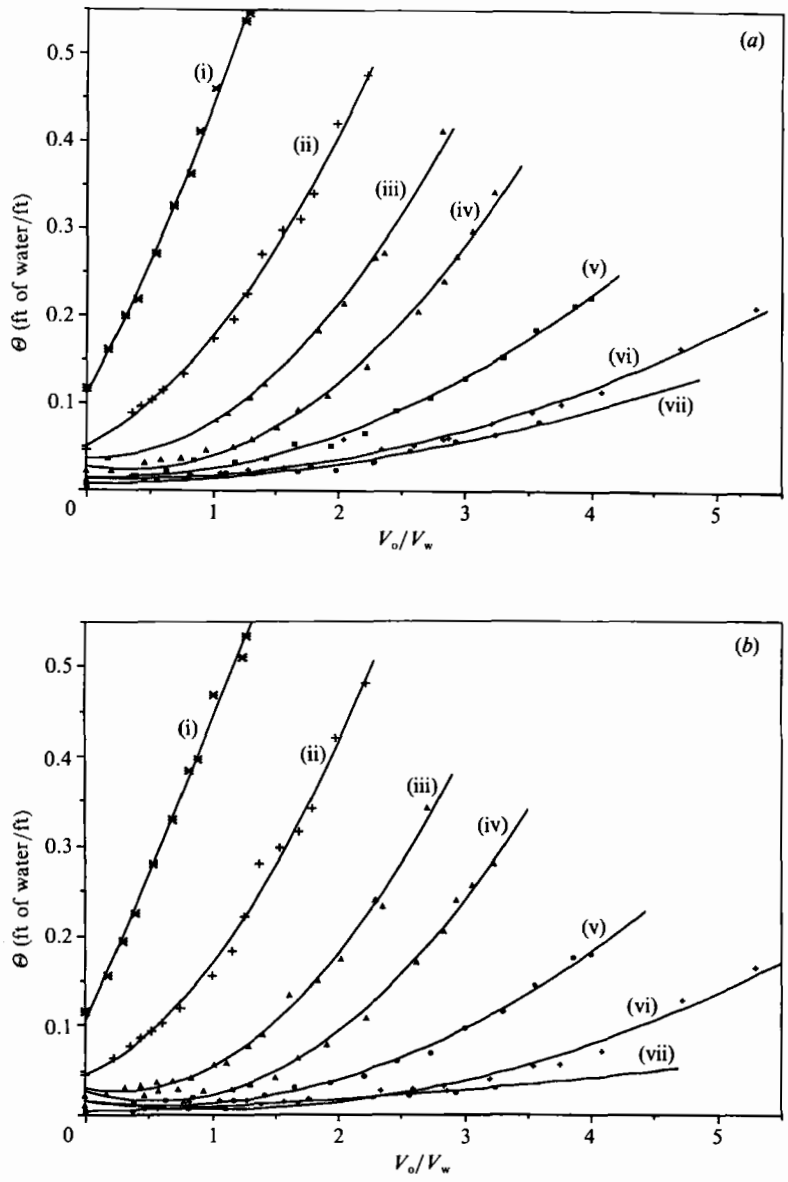

FIGURE 17. Dimensionless pressure gradient as a function of the input ratio for various values of water flow velocity V_w in ft/s: (i) 2.80, (ii) 1.08, (iii) 1.12, (iv) 0.83, (v) 0.55, (vi) 0.38, (vii) 0.33. For each V_w, Θ is an increasing function of V_o, with larger increases for larger values of V_w and no increases, even decreases, for small values of V_w. (*a*) Upflow, (*b*) downflow.

are given in figure 18. The reader's attention should focus on the following practical result: for a fixed flow rate of oil there is an optimal flow rate V_w of water, with V_w/V_o between 0.2 and 0.8 in the experiments, for which Θ is minimum. This means that the flow rates of water and oil can be adjusted to minimize energy expenditure while transporting the same amount of oil. The minimum-Θ point moves toward lower values of V_w/V_o as V_o is increased. Similar results for vertical air/water flows have been documented in figure 11.17*b* of the monograph by Wallis (1961). All the minimum points in upflow are located in regions of bamboo waves. The minimum

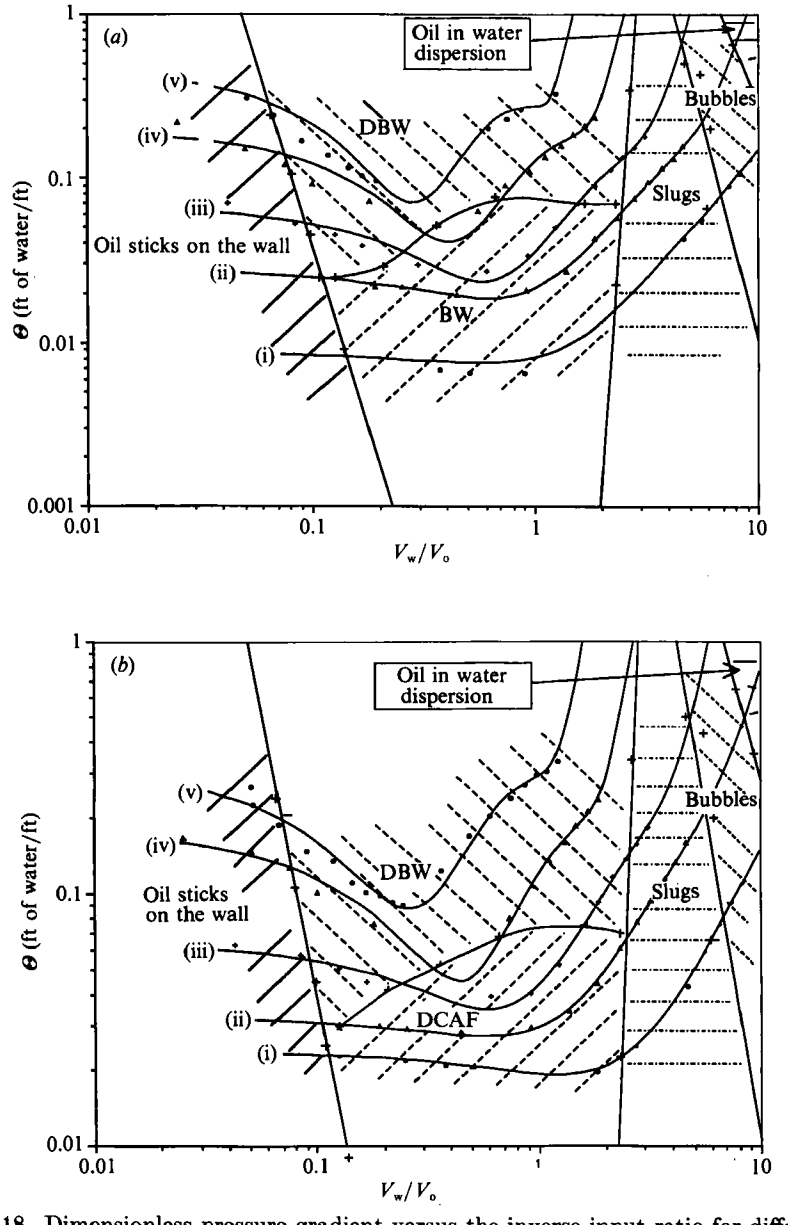

FIGURE 18. Dimensionless pressure gradient versus the inverse input ratio for different values of the oil velocity in ft/s: (i) 0.31, (ii) 0.61, (iii) 0.91, (iv) 1.51, (v) 2.27. (*a*) Upflow, (*b*) downflow.

pressure gradients fall in the region of DCAF. In this region one finds corkscrew waves, PCAF or nearly PCAL with disturbances in the form of immature corkscrew waves, or bamboo waves.

7. Ideal and measured efficiency of water lubrication

To assess the energy saving due to water lubrication in vertical flow, we compared measured values of the flow rates, holdup ratio and pressure gradients with certain

ideal values computed in different ways which are described below. The ideal values are determined by the solutions of the equation

$$-\hat{P}' + \rho_l g + \mu_l (W'' + 1/r\, W') = 0 \tag{7.1}$$

for $W = W_l(r)$ which holds for upflow in the region $l = 1$ of the core $0 < r < R_1$ and the region $l = 2$ of the annulus $R_1 < r < R_2$ (see CBJ) when

$$\frac{\mathrm{d}\hat{P}_1}{\mathrm{d}x} = \frac{\mathrm{d}\hat{P}_2}{\mathrm{d}x} = \hat{P}',$$

is one and the same constant pressure gradient. In (7.1) $W(r)$ is the axial velocity of PCAF, and μ is viscosity.

If we think of x increasing in the same direction as gravity, we have the same equation (7.1) as in upflow but with velocities reversed. The equations derived below are for downflow, and the equations for upflow can be obtained by changing the sign of velocities.

The solution of (7.1) together with appropriate boundary and interface conditions stated by CBJ is

$$W_1(r) = \frac{f_1}{4\mu_1}(R_1^2 - r^2) + \frac{f_2}{4\mu_2}(R_2^2 - R_1^2) + \frac{R_1^2 [\![\rho]\!] g}{2\mu_2} \ln \frac{R_2}{R_1} \tag{7.2}$$

and

$$W_2(r) = \frac{f_2}{4\mu_2}(R_2^2 - r^2) - \frac{R_1^2 [\![\rho]\!] g}{2\mu_2} \ln \frac{r}{R_2}. \tag{7.3}$$

Here

$$\left.\begin{aligned} f_1 &= -\hat{P}' + \rho_1 g = -p' + (\rho_1 - \rho_c) g = -p' + (1-\eta^2)\,[\![\rho]\!]\, g, \\ f_2 &= -\hat{P}' + \rho_2 g = -p' + (\rho_2 - \rho_c) g = -p' - \eta^2 [\![\rho]\!]\, g, \end{aligned}\right\} \tag{7.4}$$

where p' is obtained from the dynamic pressure p which we measure by the method of §2 $\eta = 1/a$ and

$$\rho_c = (1-\eta^2)\rho_2 + \eta^2 \rho_1, \tag{7.5}$$

where $\rho_2 = \rho_w$ and $\rho_1 = \rho_o$. The $[\![\ ]\!]$ denote a jump at the oil–water interface.

The oil flow rate is given by

$$\begin{aligned} Q_1 &= 2\pi \int_0^{R_1} r W_1(r)\, \mathrm{d}r \\ &= 2\pi \left\{ \frac{f_1}{16\mu_1} R_1^4 + \frac{f_2}{8\mu_2}(R_2^2 R_1^2 - R_1^4) + \frac{R_1^4 [\![\rho]\!] g}{4\mu_2} \ln \frac{R_2}{R_1} \right\}. \end{aligned} \tag{7.6}$$

The flow rate is given by

$$\begin{aligned} Q_2 &= 2\pi \int_{R_1}^{R_2} r W_2(r)\, \mathrm{d}r \\ &= 2\pi \left\{ \frac{f_2}{16\mu_2}(R_2^2 - R_1^2)^2 + \frac{[\![\rho]\!] g}{8\mu_2} \left[R_1^2 R_2^2 + 2R_1^4 \ln \frac{R_1}{R_2} - R_1^4 \right] \right\}. \end{aligned} \tag{7.7}$$

When the only oil is in the pipe, $R_1 = R_2$, $Q_2 = 0$, $f_1 = -p'$. When only water is in the pipe, $R_1 = 0$ and $Q_1 = 0$, $f_2 = -p'$. Hence in both cases

$$Q = -p'/8\mu\pi R_2^4. \tag{7.8}$$

When $g = 0$, the case of matched densities studied by CGH, we have

$$Q_1 = -\frac{p'\pi R_1^4}{8\mu_1}\left\{1+2\frac{\mu_1}{\mu_2}\left(\frac{R_2^2}{R_1^2}-1\right)\right\} \tag{7.9}$$

and

$$Q_2 = \frac{-p'\pi}{8\mu_2}(R_2^2-R_1^2)^2. \tag{7.10}$$

We may define various optimization problems using these formulae. For example, Joseph *et al.* (1984*b*) found the water fraction, the value of R_1 such that the total volume flux Q_1+Q_2 is maximum among all the flows satisfying (7.9) and (7.10) for a given pressure gradient p'. Another problem is to maximize Q_1 alone under the same conditions. This is a payoff calculation in which the water fraction is chosen to maximize the throughput of oil. This problem was solved when $[\![\rho]\!]\, g = 0$ by Russell & Charles (1959) and their solution was derived again by Joseph, Nguyen & Beavers (1984*a*).

The slightly more difficult case of vertical upflow is considered below. First we rewrite (7.6) and (7.7) in a more convenient form in which we introduce the superficial velocities $V_o = Q_1/\pi R_2^2$ and $V_w = Q_2/\pi R_2^2$. Thus

$$(4V_o\mu_2/R_2^2 g) = -p'/g\{\tfrac{1}{2}m\eta^4+\eta^2-\eta^4\}+[\![\rho]\!]\{\tfrac{1}{2}m(\eta^4-\eta^6)-\eta^4+\eta^6-2\eta^4\ln\eta\} \tag{7.11}$$

and

$$(4V_w\mu_2/R_2^2 g) = -p'/2g(1-\eta^2)^2+\tfrac{1}{2}[\![\rho]\!]\{\eta^2-\eta^6+4\eta^4\ln\eta\}, \tag{7.12}$$

where $m = \mu_2/\mu_1$. Equations (7.11) and (7.12) each depend on two dimensionless parameters and the right-hand sides of both depend on one parameter $p'/g[\![\rho]\!]$, which is positive as $p' < 0$, $[\![\rho]\!] < 0$ in our flows. The same formulae hold in upflow with the sign of g reversed.

A theoretical formula for the holdup ratio can be derived from (3.1), (3.2), (7.11) and (7.12):

$$\begin{aligned} h &= V_o H_w/V_w H_o \\ &= 2\frac{(1-\eta^2)\{\Theta(\tfrac{1}{2}m\eta^4+\eta^2-\eta^4)+([\![\rho]\!]/\rho_w)[(\tfrac{1}{2}m-1)(\eta^4-\eta^6)-2\eta^4\ln\eta]\}}{\eta^2\{\Theta(1-\eta^2)^2+([\![\rho]\!]/\rho_w)(\eta^2-\eta^6+4\eta^4\ln\eta)\}}, \end{aligned} \tag{7.13}$$

where

$$(-p'/\rho_w g) \overset{\text{def}}{=} \Theta \tag{7.14}$$

is a dimensionless pressure gradient which can be compared with $\Delta p/\rho_w gL$ measured in experiments.

The maximization problem solved by Russell & Charles (1959) is to maximize V_o with respect to η, for fixed p' when $[\![\rho]\!] = 0$. They found that V_o is maximum when

$$\eta = (1/2-m)^{\frac{1}{2}}.$$

In our experiments

$$m \approx 1/601, \quad [\![\rho]\!]\, g = -0.090g$$

and the oil flow–pressure gradient relation (7.11) for downflow becomes

$$\frac{4V_o\mu_2}{R_2^2 g\rho_w} = -\frac{p'}{g\rho_w}(\eta^2-\eta^4)-\frac{0.090}{\rho_w}(\eta^6-\eta^4-2\eta^4\ln\eta) \tag{7.15}$$

where $\rho_w = 0.995$, to within a small error. The same formula holds in upflow with the signs of V_o and V_w reversed.

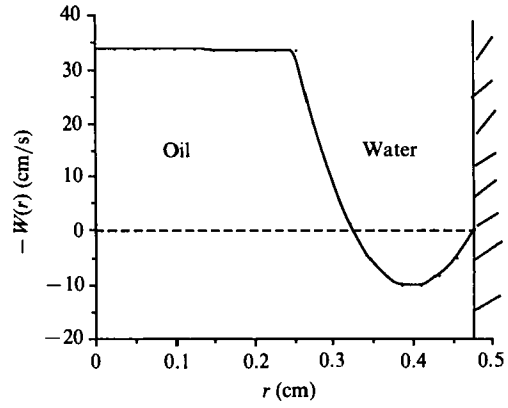

FIGURE 19. Upflow with negative flow of water. $V_o = -0.305$ ft/s, $V_w = 0.046$ ft/s.

Exp. no.	V_{oe}	V_{we}	η_e	Flow type	h_e	Θ_e	η	$\Theta_L(\eta)$	$h_L(\eta)$
1	0.305	0.554	0.53	BW	1.39	0.019	0.34	0.0013	4.18
2	0.607	0.272	0.77	BW	1.39	0.020	0.56	−0.004	4.83
3	0.909	0.554	0.80	BW	1.39	0.027	0.58	0.003	3.31
4	1.513	0.445	0.83	BW	1.39	0.052	0.72	0.016	2.53
5	2.269	0.494	0.88	DBW	1.39	0.096	0.82	0.044	2.19
6	0.305	0.554	0.59	DCAF	1.39	0.020	0.61	0.026	1.59
7	0.607	0.154	0.85	DCAF	1.39	0.025	0.85	0.028	1.59
8	0.909	0.154	0.80	DCAF	1.39	0.033	0.88	0.038	1.78
9	1.513	0.554	0.83	DCAF	1.39	0.052	0.78	0.050	1.72
10	2.269	0.554	0.86	DBW	1.39	0.090	0.83	0.071	1.86

Exp. no.	$Q_L(\eta_e)$	$V_{wL}(\eta_e)$	$h_L(\eta_e)$	$\eta_m(\Theta_e)$	$V_{oL}(\Theta_e)$	$V_{wL}(\Theta_e)$	$h_L(\eta_m)$	$\Theta_L(1)$	$\Theta_L(0)$
1	−0.011	−0.046*	−16.7	0.67	1.68	0.82	2.53	2.34	0.0095
2	−0.000 13	0.11	3.89	0.67	1.73	0.84	2.51	4.65	0.0097
3	0.003 8	0.25	2.97	0.67	2.04	1.01	2.41	6.96	0.016
4	0.026	0.31	2.29	0.68	3.17	1.60	2.24	11.6	0.023
5	0.062	0.31	2.11	0.69	5.16	2.61	2.141	7.4	0.031
6	0.027	0.64	0.91	0.89	0.34	0.06	1.55	2.34	0.0095
7	0.028	0.14	1.61	0.86	0.50	0.11	1.57	4.65	0.0084
8	0.04	0.12	1.84	0.82	0.81	0.24	1.62	6.96	0.012
9	0.051	0.45	1.76	0.77	1.61	0.65	1.72	11.6	0.023
10	0.076	0.41	1.90	0.74	3.31	1.53	1.84	17.4	0.031

TABLE 1. Comparison of experimental and ideal values in upflow (1–5) and downflow (6–10) for the same oil flow. V is given in ft/s. The other quantities are dimensionless. *The velocity profile for this case of negative V_w is shown in figure 19.

In the first five rows of table 1 we compare experimental and ideal results for five cases of upflow, and in rows 6–10 for five cases of downflow. The columns of this table are as follows: V_{oe} is the superficial velocity from experiments, V_{we} the prescribed water velocity, h_e is the holdup ratio from figure 5, $\eta_e = R_{1e}/R_2$ is the experimental ratio of the mean radius of the interface to pipe radius which is computed from h_e, using (3.4), and Θ_e is the measured value of dimensionless pressure gradient. The case of negative V_w for case 1 shown on the table is plotted in figure 19. We may define an ideal flow as PCAF satisfying (7.11) and (7.12). Then η, $\Theta_L(\eta)$ are computed from (7.11) and (7.12) when $(V_o, V_w) = (V_{oe}, V_{we})$ and (7.13) determines $h_L(\eta)$. $\Theta_L(\eta_e)$, $V_{wL}(\eta_e)$

Exp. no.	Flow type	$\Theta_L(1)/\Theta_e$	$\Theta_L(\eta)/\Theta_e$	$\Theta_L(\eta_e)/\Theta_e$	$\Theta_L(0)/\Theta_e$	$\mathbb{R}_V$
1	BW	122.93	0.068	−0.58	0.49	2481
2	BW	232.46	−0.20	−0.0065	0.49	2599
3	BW	257.88	0.11	0.14	0.60	4226
4	BW	222.87	0.31	0.50	0.44	5656
5	DBW	180.97	0.46	0.65	0.32	7981
6	DCAF	116.79	1.30	1.35	0.47	2481
7	DCAF	185.97	1.12	1.12	0.34	2198
8	DCAF	210.99	0.85	1.21	0.36	3071
9	DCAF	222.88	0.96	0.98	0.44	5971
10	DBW	193.04	0.79	1.07	0.35	8155

TABLE 2. Comparison of the ratio of the ideal to the experimental pressure gradients for the same oil flow. The Reynolds number $\mathbb{R}_V = (V_o + V_w)d/\nu_w$. When $\mathbb{R}_V > \mathbb{R}_{Vc}$ where $\mathbb{R}_{Vc} \approx 2000$, the flow is turbulent. In the turbulent case we should replace $\Theta_L(0)$ with $\Theta_T(0) > \Theta_L(0)$ because a greater pressure gradient is required for the same volume flux in turbulence flow.

and $h_L(\eta_e)$ are computed from the formulae when $(\eta, V_o) = (\eta_e, V_{oe})$ are given. The value $\eta = 1/\sqrt{2}$ is a good approximation to the value of η which minimizes $\Theta(\eta) = -p'/g\rho_w$ for a fixed value of V_o. We can prove this when η is close to one by noting that

$$\begin{aligned}\eta^6 - \eta^4 - 2\eta^4 \ln \eta &= \eta^6 - \eta^4 - \eta^4 \ln [1 - (1-\eta^2)] \\ &= \eta^6 - \eta^4 + \eta^4(1-\eta^2) + O[(1-\eta^2)^2] \\ &= O[(1-\eta^2)^2]. \end{aligned} \tag{7.16}$$

The result $\eta = 1/\sqrt{2}$ follows from (7.15) when the second term of the right-hand side is zero. $\eta_m(\Theta_e)$ is the value of η which maximizes $V_o = V_{oL}(\Theta_e)$ in (7.11) when $\Theta = \Theta_e$, and $h_L(\eta_m)$ is calculated from (7.13) with $(\eta, \Theta) = (\eta_m, \Theta_e)$.

The value $\Theta(1)$ is the dimensionless pressure gradient required to transport oil alone in the same pipe with the same oil throughput. We obtain

$$\Theta(1) = 8V_o\mu_1/gR_2^2\rho_w \tag{7.17}$$

from (7.11) with $\eta = 1$.

Another measure of efficiency which is used in the oil industry is to compare the observed pressure gradient Θ_e with the pressure drop $\Theta(0)$ required to transport water alone with a volume flux $Q_{o+w} = Q_o + Q_w$ equal to the total flux. We can compute $\Theta_L(0)$ for the laminar flow of water from (7.8):

$$\Theta_L(0) = \frac{8V_{o+w}\mu_2}{gR_2^2\rho_w} \text{(laminar)}, \tag{7.18}$$

where $V_{o+w} = V_o + V_{we} = Q_{o+w}/A$ can be obtained from tables.

In table 2 we show various pressure gradient ratios, which are measures of efficiency together with the values of the Reynolds number

$$\mathbb{R}_V = \frac{V_{o+w}d}{\nu_w}, \quad \nu_w = \frac{\mu_2}{\rho_w},$$

where $d = \frac{3}{8}$ in. and $\mu_2 = 10^{-2}$ P. Hence

$$\mathbb{R}_V = V_{o+w}\, 12(2.54)^2\, 300/8 \approx 2903\, V_{o+w}. \tag{7.19}$$

For $\mathbb{R}_V > 2300$ we should not compare Θ_e with $\Theta_L(0)$ for laminar flow. For these, we should compute $\Theta_T(0)$, the pressure gradient for turbulent flow at a superficial velocity of V_{o+w}, which is greater; $\Theta_T(0) = k\Theta_L(0)$ with $k > 1$. For example, $k = \frac{3}{2}$, to transport a given mass flux in turbulent flow. So as a rough measure the reader should reduce the number $\Theta_L(0)/\Theta_e$ by $\frac{2}{3}$ when $\mathbb{R}_V > 2300$. In this way we may understand how it can happen that the pressure gradient required to drive oil plus water in the lubricated pipeline can be smaller than the pressure gradient required to drive the same flux of water alone.

From our comparisons of ideal and measured values of the pressure gradients we may draw the following conclusions.

(i) The pressure drops required to transport a given flux of oil with water lubrication are about 200 times less than the pressure drops required to transport the same flux of 601 cP oil without lubrication. In general, in vertical pipes we expect a reduction of the order k/m where $m = \mu_2/\mu_1$ and k is a fraction, say about $\frac{1}{3}$.

(ii) The pressure drops required to transport a given flux of oil and water with water lubrication is of the same order as, and can be even less than, the pressure drop necessary to transport water alone at a superficial velocity V_{o+w} corresponding to the total flux, provided that V_{o+w} is such that $\mathbb{R}$ given by (7.19) is greater than 2300. In this case the pressure drop in the water alone is computed for turbulent flow.

(iii) Bamboo waves require a much greater pressure gradient to transport a given volume flux of oil at low oil velocity and fixed water velocity than in the ideal case. This comparison is not interesting because its significance is diminished by the fact that oil is usually being transported by buoyancy.

(iv) Disturbed core–annular flow with corkscrew waves is energy efficient, with pressure gradients only moderately greater, sometimes even less, than those required for perfect core–annular flow with the same water fraction. This shows that DCAF is close to PCAF.

8. Comparison of experiments with the linear theory of stability

We computed results from the linear theory of stability using the equations of CBJ. Their Reynolds number is defined as $\mathbb{R}_g(R_1) = W_g R_1/\nu_1$, where $W_g = gR_1^2/\nu_1$ and $F = -\hat{P}'/\rho_1 g$ is also prescribed in the computations of CBJ. Lengths are scaled with R_1, velocity with W_g and time with R_1/W_g. CBJ took x increasing in the direction of gravity so that $W(r)$ in upflow in this paper is $-W(r)$ in CBJ.

We did two kinds of comparisons of theory and experiments. First, we calculated wavelengths and wave speeds in the regions of parameter space in which waves were observed and compared the calculated and measured values. Secondly, we tried to determine the regions of parameter space where different flow types could be found by analysis of the energy of the most dangerous disturbance.

It is useful here to draw attention again to the fact that we are trying to compare results of a linear theory of stability of PCAF with flow types in deeply nonlinear regions of flow. There are different ways to make this comparison corresponding to different choices of the laminar flow which is supposed to be relevant for the nonlinear flow which is observed. We shall give a more precise characterization of the possible choices below.

A laminar flow is determined by two parameters, say V_w and V_o, or V_o and $a = 1/\eta = R_2/R_1$, or V_w and a. For example, given V_o and V_w we may compute η and p' from (7.11) and (7.12). We may conclude that other types of flow, say bamboo waves, are determined by prescribing two parameters plus the flow type. We choose

	Experiments		Computations		
Exp. no.	λ (cm)	c (cm/s)	λ (cm)	c (cm/s)	$W(1)$ (cm/s)
1	1.21	57.70	0.82 (0.79)	79.84 (52.02)	83.69 (55.64)
2	1.31	43.28	0.92 (0.96)	80.21 (42.54)	83.73 (46.24)
3	1.41	35.65	1.22 (1.22)	79.76 (33.51)	82.91 (37.26)
4	1.22	27.81	1.65 (1.33)	77.00 (29.42)	79.94 (32.66)
5	1.374	19.16	1.56 (1.25)	58.91 (17.94)	62.05 (20.75)
6	1.79	22.90	1.23 (1.16)	58.12 (22.17)	61.69 (25.35)
7	1.34	28.22	1.05 (1.02)	54.80 (26.68)	58.49 (29.95)
8	1.17	31.06	0.95 (0.87)	50.85 (31.33)	54.58 (34.53)
9	0.90	36.25	0.86 (0.79)	49.38 (35.71)	53.01 (39.12)

TABLE 3. Comparison of computed and measured values of the wave speed c and wavelength λ of bamboo waves at the flow points 1–9 of the flow chart in figure 13 for upflow. The speed $W(1)$ of the undisturbed interface is also listed. The computations are for the most unstable mode. The values listed in the parentheses are those computed when V_o, $a = a_e$ are prescribed.

to make our comparisons for all flow types having: (i) the same oil and water inputs, that is V_o and V_w are prescribed and equal to measured values; and (ii) the same oil input, V_o and the same water fraction expressed by $a = a_e$, where a_e is taken from the measured holdup $h = h_e$ in figure 5. Bamboo waves trap water between the crests (see figure 8) and sweep it through the system faster than in laminar flow: less water is held up. Then $\eta_e > \eta$ or $a_e < a$ in upflow. In downflow this trapping does not operate and the experimental holdup is nearly the same as the laminar one (see table 1).

8.1. *Comparison of linear theory with experiments for fixed values of V_o and V_w*

Calculations were carried out for the emulsified oil used in the experiments at a temperature of 22 °C with material parameters given by (2.1). The dimensionless parameters are

$$m = 1/601 = 1.66 \times 10^{-3}, \quad \rho_w/\rho_o = 0.995/0.905 = 1.10, \quad J^* = TR_2/(\rho_o \nu_o^2) = 0.102, \tag{8.1}$$

where T is interfacial tension and ν_o the oil kinematic viscosity. In our first comparison of linear theory with experiments, we select nine arbitrary cases of bamboo waves from experiments and compare observed and calculated wavelengths and wave speeds. Bamboo waves are imperfectly periodic but it is easy to identify average values, taken as simple averages from video recordings using scaled reticle and automatic lapsed-timer features of SPIN PHYSICS2000. To compute wavelengths and wave speed from linear theory, we need to identify the unstable wave of maximum growth. For this it is sufficient to prescribe two values $(Q_o, Q_w) = (V_o, V_w)A$. Then the parameters a, F and $\mathbb{R}_g$ can be computed from the PCAF formulae in §7; values of the oil and water volume flow rates $Q_o = V_o A$ and $Q_w = V_w A$ are prescribed.

8.1.1. *Upflow*

The comparison of computed and measured values of the wave speed and wavelength of bamboo waves for points 1–9 of figure 13 is given in table 3. The measured values of the wavelength are on average slightly larger than computed values, probably due to the nonlinear stretching associated with the lubrication and buoyancy effects described in figure 8.

Exp. no.	$\mathring{E}$	$I-D$	B_1	B_2	B_3
1	0.1836 (0.1552)	−0.7932 (−0.8241)	−0.01419 (−0.01659)	0.9944 (0.9961)	−0.00359 (−0.00284)
2	0.2142 (0.2117)	−0.7680 (−0.7511)	−0.01080 (−0.01409)	0.9983 (0.9818)	−0.00544 (−0.00497)
3	0.2759 (0.3352)	−0.7081 (−0.6131)	0 (−0.00851)	0.9950 (0.9659)	−0.01123 (−0.00915)
4	0.3480 (0.4186)	−0.6332 (−0.5502)	0.01423 (−0.00451)	0.9873 (0.9848)	−0.02057 (−0.01150)
5	0.3837 (0.3491)	−0.5869 (−0.6323)	0.00830 (−0.01078)	0.9800 (1.0013)	−0.01781 (−0.00918)
6	0.3133 (0.2463)	−0.6485 (−0.7165)	−0.00321 (−0.01238)	0.9754 (0.9828)	−0.01062 (−0.00772)
7	0.2640 (0.1805)	−0.6996 (−0.7826)	−0.00968 (−0.01422)	0.9802 (0.9829)	−0.00700 (−0.00558)
8	0.2244 (0.1402)	−0.7405 (−0.8303)	−0.01329 (−0.01603)	0.9833 (0.9902)	−0.00514 (−0.00371)
9	0.1829 (0.1203)	−0.7881 (−0.8487)	−0.01554 (−0.01584)	0.9903 (0.9876)	−0.00378 (−0.00271)

TABLE 4. Energy budget for equation (8.2) evaluated on the most unstable mode at each of 9 points labelled in figure 13. Positive values of $\mathring{E}$ mean that PCAF is unstable. The values listed in parentheses are those computed when V_0, $a = a_e$ are prescribed. The flows are all unstable to interfacial friction, $B_2 > 0$, leading to bamboo waves.

The speed $W(1)$ of the undisturbed interface is on average slightly larger than the computed value of c. This shows that the bamboo wave is on average basically stationary in a frame moving with velocity $W(1)$. As a further check we computed $c = 8.03$ cm/s, $W(1) = 9.84$ cm/s at point D2 on figure 13 and $c = 16.96$ cm/s, $W(1) = 18.95$ cm/s at E2. The viscosity of the oil is too large to support any but slowly propagating waves, so the wave is convected with the oil. Analysis of the singular problem $m \to 0$ by Hu *et al.* (1990) shows that $c \to W(1)$ in the limit $m \to 0$.

The discrepancy between the computed and measured values of the wave speed is consistent with the idea that the wave is convected with the oil. The reason for the discrepancy can be traced to the fact that the water fraction for laminar flow with V_o, V_w prescribed is larger than the measured water fraction in upflow; $\eta < \eta_e$ in the first five columns of table 1. Since V_o is prescribed, and of the same value in laminar flow and bamboo waves, the oil in a core with $R_1 < R_{1e}$ must flow faster. Hence the speed discrepancy between c in theory and experiments is due to the reduction of the water fraction due to sweep-out effects of bamboo waves.

We turn next to analysis of the equation governing the evolution of the kinetic energy E of the most unstable disturbance of PCAF. This may be written as

$$\mathring{E} = I - D + B_1 + B_2 + B_3, \tag{8.2}$$

where $I-D$ is the Reynolds stress minus the dissipation (and we normalize with $D = 1$), B_1 is a boundary term associated with interfacial tension, B_2 is a boundary term associated with the viscosity difference which we call interfacial friction, and B_3 is a boundary term in the energy supply which is proportional to gravity times the jump in density. Table 4 shows that, according to the maximum growth rate criterion of linear theory, bamboo waves are driven by interfacial friction; the other terms in the energy equation are stabilizing with very slight destabilizing effect from interfacial tension in experiments 4 and 5.

Energy-budget terms for the other labelled points in the upflow chart of figure 13 are displayed in table 5. In addition, we have given the value of the wavelength $\hat{\lambda} = 2\pi/\hat{\alpha}$ of the fastest growing wave. PCJ showed that the length of the slugs and bubbles which are observed correlate well with $\frac{1}{2}\hat{\lambda}$. We would not get this kind of agreement here, because the slugs are stretched and stringy due to buoyancy and shear (see figure 6). We have a good agreement between theory and experiment with regard to selection of flow type in a sense which needs explanation. In all the entries the Reynolds stress term $I-D$ is stabilizing. Hu & Joseph (1989*a*) showed that when the flow is unstable $\mathring{E} > 0$ and $I-D > 0$ is destabilizing (all other terms negative), correlating with transitions to w/o (water into oil) emulsions, in the experiments of CGH and in field tests, using privileged data. We have no budget which should lead to w/o dispersions and none are observed. In every case where slugs, bubbles and o/w dispersions are observed, PCAF is unstable both to interfacial tension B_1 and interfacial friction B_3; the other terms are stabilizing. The size of the bubbles in the o/w dispersions is much smaller than $\frac{1}{2}\hat{\lambda}$ and is probably associated with the breakup of large bubbles in shear flow.

The energy budgets for the cases of bamboo waves and disturbed bamboo waves that are observed are all alike. The instability producing these waves is due to a strongly positive B_2, with all other effects being stabilizing or at least only weakly destabilizing. Interfacial friction drives interfacial waves.

Points	$\hat{E}$	$I-D$	B_1	B_2	B_3	$\hat{\lambda}$ (cm)	Flow region in the chart
A1	0.2450	−0.8982	0.4145	0.7341	−0.0060	1.5519	o/w dispersion
B1	0.2852	−0.8791	0.2085	0.9702	−0.0148	1.7295	oil bubble
C1	0.3052	−0.8610	0.1362	1.0485	−0.0189	1.7833	oil bubble
D1	0.4116	−0.6853	0.0388	0.0816	−0.0237	1.8341	BW/slug
E1	0.4264	−0.5353	0.0011	0.9798	−0.0141	1.4624	oil sticks on the pipe wall
F1	0.0032	−0.9954	−0.0021	0.9978	−0.0001	0.2342	oil sticks on the pipe wall
A2	0.2291	−0.9038	0.4840	0.6532	−0.0053	1.5268	o/w dispersion
B2	0.2719	−0.8862	0.2387	0.9331	−0.0143	1.7116	oil bubble
C2	0.3424	−0.8050	0.0909	1.0806	−0.0243	1.9188	oil slug
D2	0.4566	−0.5449	0.0167	1.0068	−0.0220	1.7690	BW
E2	0.2814	−0.6791	−0.0120	0.9799	−0.0075	1.1267	BW
F2	0.0552	−0.9261	−0.0115	0.9968	−0.0001	0.2604	oil sticks on the pipe wall
A3	0.0742	−0.9778	1.1728	−0.1204	−0.0012	1.0009	o/w dispersion
B3	0.1353	−0.9530	0.7341	0.3618	−0.0084	1.3061	o/w dispersion
C3	0.2721	−0.8208	0.1095	1.0203	−0.0373	2.1226	oil bubble
D3	0.2983	−0.7031	0.0221	1.0022	−0.0231	1.6892	oil slug
E3	0.2457	−0.7436	0.0030	0.9980	−0.0119	1.2353	BW
F3	0.1371	−0.8506	−0.0158	1.0049	−0.0014	0.6096	DBW

TABLE 5. Energy budget for equation (8.2) evaluated on the most unstable mode at labelled points in figure 13. $\hat{\lambda}$ is the dimensional wavelength based on the most unstable mode.

Points	$\hat{E}$	$I-D$	B_1	B_2	B_3	$\hat{\lambda}$ (cm)	Flow region in the chart
1	0.1690	−0.8327	0.0035	1.2220	−0.2238	13.4382	slugs
2							DCAF
			stable				
3							DCAF
4	0.0854	−0.9150	−0.0126	1.0085	0.0002	0.2887	DBW

TABLE 6. Energy budget for equation (8.2) evaluated on the most unstable mode at labelled points in figure 15. $\hat{\lambda}$ is the dimensional wavelength based on the most unstable mode.

8.1.2. *Downflow*

For downflow, we compare theory and experiment at four arbitrarily chosen points on the downflow chart in figure 15. The flows at points in the DCAF region are essentially PCAF as the theory predicts (see table 6). Point 4 in the region of disturbed bamboo waves is unstable to interfacial friction. Point 1 in the region of slugs is also unstable to interfacial tension. This gives perfect agreement at all four points.

8.2. *Comparison of linear theory with experiment for fixed values of V_0 and a*

We remarked that the discrepancy between the theoretical and measured values of c in table 3 was due to the sweeping out of trapped water between the crests of bamboo waves leading to a reduced water fraction. To check this idea, we decided to compute stability results when V_0 is prescribed as in the experiment and $a = a_e$ is given by experiment. This ideas is completely consistent with results shown in parentheses in table 3. The energy decomposition shown in parentheses in table 4 is also completely consistent with the idea that bamboo waves are produced by interfacial friction.

We carried out a similar computation, with V_0, a_e prescribed, but with parameters appropriate to pure oil. We got agreement between theory and experiments even though the oil used in the experiments is not the one used in the theory. In fact many results are insensitive to small changes of viscosity when the water fraction is fixed.

9. Summary and discussion

We have reported the results of experiments on water-lubricated pipelining of 6.01 P cylinder oil in a vertical apparatus with up- and downflow. The measurements were compared with theoretical predictions based on ideal laminar flow (PCAF) and with the linear theory of stability. Flow rates for the oil and water, pressure gradients and holdup ratios for up- and downflow over a wide range of velocities less than 3 ft/s were recorded.

The oil is buoyed up in water by gravity. In upflow the pressure gradient and buoyancy are in the same direction. Waves develop in upflow and the lubrication forces together with the buoyancy tend to stretch wave troughs. In downflow the pressure gradient and buoyancy are opposed. This compresses the oil column, suppresses bamboo waves, and leads to straight or buckled columns of oil. The differences between up- and downflow are suppressed in fast flow when the pressure gradient dominates buoyancy. The stretching of oil in upflow and its compression in downflow implies that less oil will accumulate in upflow than in downflow. It is possible to fluidize hugely long slugs of oil in downflow.

The ratio of the input ratio to the volume ratio is called the holdup ratio h, which is one in a well-mixed flow and larger than one in a laminar lubricated flow without gravity. Buoyancy changes this; zero and even negative holdups are possible (see figure 19).

Different types of flow were observed and located on flow charts in a (V_w, V_o)-plane. The flow types change with the oil flow at a fixed water flow.

First we describe changes in upflow as the oil flow is increased. For slow oil flow with enough water, oil bubbles will form by capillary instability; if the water flow is fast enough the large bubbles are torn apart, leaving o/w dispersions. When the water flow is slow enough to support capillary bubbles, increasing oil flow will cause the bubbles to connect into longer structures, called slugs, which are like segments of bamboo with bamboo swells connected by long thin bamboo stems. Further increases in the oil flow cause the segments to connect into a definite bamboo train. The stems of the bamboo thicken and the distance between the cells decreases with increasing oil flow. Bamboo waves seem to be imperfect monochromatic waves with a very well-defined average length, speed and amplitude. Yet further increases in the oil throughput lead to much thicker and shorter stems and the bamboo crests become very jagged, irregularly not axisymmetric. These are called disturbed bamboo waves and, like bamboo waves, are robust regimes of upflow.

In a certain region of the upflow chart, small water flow and large oil flow, the oil sticks to the wall. This is a flow-induced adhesion, and it can be reversed. This flow induced 'change of adhesion' results either in blockage with a loss of lubrication or in a three-layer configuration with oil on the outer wall, water in an annulus beneath and oil in the core. Our apparatus could not withstand the pressures needed to produce larger rates of oil flow than in the ones in which oil sticks to the wall. We believe that water-in-oil emulsions would arise if the oil flow could be increased.

Now we describe downflow after the flow turns at the bend at the upper end of the pipe, first for high oil flows with disturbed bamboo waves in upflow and then as the oil

flow is decreased. When such waves are observed at high oil flow rates in upflow, they are also observed in downflow. However, their wavelengths are shorter in downflow because of stretching in upflow and compression in downflow. When the oil input is decreased the waves disappear, leading to DCAF. This flow can be almost a PCAF. At higher flow rates of oil, it is disturbed by immature bamboo waves, at lower flow rates by rotating buckled structures which we call corkscrews. At yet lower oil inputs the oil column will break into trains of long slugs and then into trains of large bubbles which seem tied together by wake forces.

For a fixed flow of oil, there is an optimum flow rate of water for which the pressure gradient is a minimum. The minimum pressure gradient is in a region of bamboo waves in upflow and in a region of disturbed core–annular flow in downflow. The pressure gradients in downflow are less than in upflow. This shows that DCAF is more efficient than bamboo waves.

Some new formulae for PCAF are derived and used to compare ideal lubrication theory with experiments and to obtain some measures of energy efficiency. To make the dynamic pressure gradient appear explicitly, it is necessary to take account of the overburden based on the composite water–oil density. There is no static solution of the PCAF problem, so that the treatment of hydrostatic gradients requires thought, and it leads to the decomposition of the governing equations in which the density appears only in terms of the density difference $[\![\rho]\!]$, as expected. These equations are easily integrated and all quantities can be evaluated on this PCAF solution when two parameters, like flow input of oil and water, are prescribed. A theoretical formula for the holdup is derived and evaluated. We find the water fraction for the PCAF flow for which the oil flow is maximum when the pressure gradient is fixed.

We compared measured pressure gradients with different ideal pressure gradients in five cases each of upflow and downflow. The pressure gradient required to move a given flow rate of 6.01 P oil is on average 200 times greater when there is no water lubrication. This improvement is roughly one-third of the ratio $\mu_o/\mu_w = 1/m$. We can guess that drag reductions of the order $\mu_o/3\mu_w$ are possible in a vertical pipeline. For a viscous crude oil, water lubrication would reduce the pressure gradient by a factor of more than 10000.

We compared measured pressure gradients with the gradients required to move water alone with a flow rate equal to measured total flow, oil plus water. For laminar flow, the measured gradients in lubricated flow are roughly three times larger than the theoretical gradients required for laminar flow of water alone. However, at the given flow rates water would be in turbulent flow and the ratio of measured to theoretical values much closer to one.

The measured values of the pressure gradient and water fraction were compared with theoretical values computed for PCAF with the same oil and water input. The computed water fraction expressed by the radius ratio $a = R_2/R_1$ is larger than the mean values $a_e = R_2/R_{1e}$ measured in the experiments. This reduction in the water fraction in the experiments is due to the transport of water trapped between bamboo waves flushing out water, leaving a smaller water fraction behind. The computed pressure gradients in upflow at low oil flow rates is much smaller than measured values. This comparison has no significance because under these conditions the motive force of transport is buoyancy. At higher oil flow rates, the ratio of computed to measured pressure gradients is of order one, between 0.1 and 0.5.

Theoretical and measured values of the water fraction and pressure gradients in downflow are very close. This shows that realized DCAF downflows – are practically optimally efficient, with pressure-gradient reductions of the same value as PCAF

with the same water fraction. This is because DCAF is at most a perturbation of PCAF. The measured gradients of pressure are not globally optimal, however, because there is another PCAF, with a different and best water fraction, for which the pressure gradient for a given flux of oil is minimum.

We compared measured values of the speed and wavelength of bamboo waves with two different theoretical values computed from the linear theory of stability. First we compared all flows with the same oil and water input, the same V_0 and V_w, as in our experiments. In the second we compared all flows with the same oil input and water fraction, the same V_0 and a, where a was put equal to the measured value for that V_0. The second comparison was introduced to validate the following conclusion: the wave on a very viscous oil, which basically must travel with nearly uniform velocity (see figure 19), must be very nearly a standing wave, convected with the flow. A 6.01 P oil is too viscous to support fast wave propagation. In every case, the computed wave speed c of the most unstable disturbance was nearly the same as the speed W of the oil core in the basic PCAF.

The average wavelength of bamboo waves is slightly larger than the wavelength of the most unstable disturbance of a $PCAF_1$, which is a PCAF with the same V_0 and V_w as in the experiments and also of a $PCAF_2$, which as a PCAF with the same V_0 and a as in the experiments. Nonlinear effects are responsible for stretching the stems of bamboo waves, explaining the small discrepancy between linear stability theory and experiments.

There is a larger discrepancy between the measured and theoretical wave speeds for PCAF, with up to three times faster speeds found in computations. We attribute this discrepancy to a systematic difference $a-a_e > 0$ between experiments and $PCAF_1$. The wave speed must be greater for flows with more water because the oil core with superficial oil velocity V_0 has to rise faster when a is larger. Since the wave is convected with the oil, a comparison of computation with one a with another computation or experiment with another will give rise to a systematic discrepancy of the observed type. In fact this systematic discrepancy disappears when the measured speeds are compared with the ones computed for the $PCAF_2$ which has the same a.

We attempted to predict the flow types observed in experiments by identifying the source of instability in the terms of the energy equations which we computed for the most dangerous disturbance of $PCAF_1$ and $PCAF_2$. For $PCAF_1$ we found that in all cases in which oil bubbles and slugs in water were observed, the instability arises from the boundary through a combination of interfacial tension and interfacial friction. In the region where bamboo waves and disturbed bamboo waves were observed, only interfacial friction acts to produce instability either of $PCAF_1$ or of $PCAF_2$. For $PCAF_1$, analysis of downflows gives rise to the same satisfying identification of the sources of instability of slug flow and disturbed bamboo waves. In addition for the two arbitrarily chosen points near the centre of the DCAF, where nearly perfect core–annular flows are actually observed, the linear theory shows $PCAF_1$ to be stable. PCJ and Hu & Joseph (1989*a*) showed that in all cases where oil-in-water dispersions were observed, instability of PCAF arises from the Reynolds stress in the water, and not from terms at the boundary. We did not observe o/w dispersion in the experiments and no term with a Reynolds-stress-induced instability was identified in the theory.

Future work correlating stability calculations with experiments using more viscous and less viscous oils in vertical flow ought to be undertaken. It is especially important to build a robust apparatus in which the pressure gradients needed to

create o/w emulsions can be attained. The transition to o/w emulsions is a practical problem of considerable importance because it leads to a loss of lubrication in the field.

This work was supported by the Department of Energy; the Army Research Office, Mathematics; the National Science Foundation, fluid mechanics; and the Minnesota Supercomputer Institute. R.B.'s work was supported in part by the People's Republic of China. We wish to thank Mike Arney for his work on the measurement of the material parameters of the fluids used in the experiments. We are indebted to Veet Kruka and Greg Geiger, at Shell development in Houston, for sharing their knowledge of the applications side of this subject, and in general, for moral and logistical support from the beginning of our studies of lubricated pipelining.

REFERENCES

AUL, R. W. & OLBRICHT, W. L. 1990 Stability of a thin annular film in pressure-driven low Reynolds number flow through a capillary. *J. Fluid Mech.* **215**, 585.

BENTWICH, M. 1976 Two-phase axial laminar flow in a pipe with naturally curved interface. *Chem. Engng Sci.* **31**, 71.

CHARLES, M. E. 1963 The pipeline flow of capsules. Part 2: theoretical analysis of the concentric flow of cylindrical forms. *Can. J. Chem. Engng* **41**, 46.

CHARLES, M. E., GOVIER, G. W. & HODGSON, G. W. 1961 The horizontal pipeline flow of equal density of oil–water mixtures. *Can. J. Chem. Engng* **39**, 17 (referred to herein as CGH).

CHARLES, M. E. & LILLEHT, L. U. 1966 Correlation of pressure gradients for the stratified laminar–turbulent pipeline flow of two immiscible liquids. *Can. J. Chem. Engng* **44**, 47.

CHARLES, M. E. & REDBERGER, R. J. 1962 The reduction of pressure gradients in oil pipelines by the addition water: numerical analysis of stratified flow. *Can. J. Chem. Engng* **40**, 70.

CHEN, K., BAI, R. & JOSEPH, D. D. 1990 Lubricated pipelining. Part 3. Stability of core–annular flow in vertical pipes. *J. Fluid Mech.* **214**, 251 (referred to herein as CBJ).

CHEN, K. & JOSEPH, D. D. 1991 Lubricated pipelining: stability of core–annular flow. Part 4. Ginzburg–Landau equations. *J. Fluid Mech.* **227**, 587.

CHERNIKIN, V. I. 1956 Combined pumping of petroleum and water in pipes. *Trudi. Mock. Neft. inta* **17**, 101–111.

CLARK, A. F. & SHAPIRO, A. 1949 Method of pumping viscous petroleum. *US Patent No.* 2533878.

FRENKEL, A. L. 1988 Nonlinear saturation of core–annular flow instabilities. In *Proc. Sixth Symp. on Energy Engineering sciences.* Argonne National laboratory.

FRENKEL, A. L., BABCHIN, A. J., LEVICH, B. G., SHLANG, T. & SHIVASHINSKY, G. I. 1987 Annular flows can keep unstable films from breakup: nonlinear saturation of capillary instability. *J. Colloid Interface Sci.* **115**, 225.

GEMMELL, A. R. & EPSTEIN, N. 1962 Numerical analysis of stratified laminar flow of two immiscible Newtonian liquids in circular pipes. *Can. J. Chem. Engng* **40**, 215.

GLASS, W. 1961 Water addition aids pumping viscous oils. *Chem. Engng Prog.* **57**, 116.

HASSON, D., MANN, U. & NIR, A. 1970 Annular flow of two immiscible liquids. I. Mechanisms. *Can. J. Chem. Engng* **48**, 514.

HICKOX, C. E. 1971 Instability due to viscosity and density stratification in axisymmetric pipe flow. *Phys. Fluids* **14**, 251.

HOOPER, A. P. & BOYD, W. G. C. 1983 Shear flow instability at the interface between two viscous fluids. *J. Fluid Mech.* **128**, 507.

HU, H. & JOSEPH, D. D. 1989*a* Lubricated pipelining: stability of core–annular flow. Part 2. *J. Fluid Mech.* **205**, 359.

HU, H. & JOSEPH, D. D. 1989*b* Stability of core–annular flow in a rotating pipe. *Phys. Fluids* A **1**, 1677.

HU, H., LUNDGREN, T. S. & JOSEPH, D. D. 1990 Stability of core–annular flow with a small viscosity ratio. *Phys. Fluids* A **2**, 1945.

ISAACS, J. D. & SPEED, J. B. 1904 Method of piping fluids. US Patent No. 759374.

JOSEPH, D. D., NGUYEN, K. & BEAVERS, G. S. 1984*a* Non-uniqueness and stability of the configuration of flow of immiscible fluids with different viscosities. *J. Fluid Mech.* **141**, 319.

JOSEPH, D. D., RENARDY, Y. & RENARDY, M. 1984*b* Instability of the flow of immiscible liquids with different viscosities in a pipe. *J. Fluid Mech.* **141**, 309.

JOSEPH, D. D. & SAUT, J. C. 1990 Short-wave instabilities and ill-posed initial-value problems. *Theor. Comput. Fluid Dyn.* **1**, 191.

JOSEPH, D. D., SINGH, P. & CHEN, K. 1990 Couette flows, rollers, emulsions, tall Taylor cells, phase separation and inversion, and a chaotic bubble in Taylor-Couette flow of two immiscible liquids. In *Nonlinear Evolution of Spatio-temporal Structures in Dissipative Continuous Systems* (ed. F. H. Busse & L. Kramer). Plenum.

KAO, T. W. & PARK, C. 1972 Experimental investigations of the stability of channel flows. Part 2. Two-layered co-current flow in a rectangular channel. *J. Fluid Mech.* **52**, 401.

LIN, S. P. & IBRAHIM, E. A. 1990 Instability of a viscous liquid jet surrounded by a viscous gas in a vertical pipe. *J. Fluid Mech.* **218**, 641.

LOOMAN, M. D. 1916 Method of conveying oil. *US Patent No.* 1119438.

OLIEMANS, R. V. A., OOMS, G., WU, H. L. & DUŸVESTIN, A. 1985 Core–annular oil/water flow: the turbulent-lubricating model and measurements in a 2 in. pipe loop. Presented at the *Middle East Oil Technical Conf. and Exhibition, Bahrain, March 11–14, 1985*. Society of Petroleum Engineers.

OOMS, G. 1971 Fluid-mechanical studies of core–annular flow. Ph.D. thesis, Delft University of Technology.

OOMS, G., SEGAL, A., CHEUNG, S. Y. & OLIEMANS, R. V. A. 1985 Propagation of long waves of finite amplitude at the interface of two viscous fluids. *Intl J. Multiphase Flow* **9**, 481.

OOM, G., SEGAL, A., VAN DER WEES, A. J., MEERHOFF, R. & OLIEMANS, R. V. A. 1984 A theoretical model for core–annular flow of a very viscous oil core and a water annulars through a horizontal pipe. *Intl J. Multiphase Flow* **10**, 41.

PAPAGEORGIOU, D. T., MALDARELLI, C. & RUMSCHITZKI, D. S. 1990 Nonlinear interfacial stability of core annular film flows. *Phys. Fluids* A **2**, 340.

PREZIOSI, L., CHEN, K. & JOSEPH, D. D. 1989 Lubricated pipelining: stability of core–annular flow. *J. Fluid Mech.* **201**, 323 (referred to herein as PCJ).

RANGER, K. B. & DAVIS, A. M. 1979 Steady pressure driven two-phase stratified laminar flow through a pipe. *Can. J. Chem. Engng* **57**, 688.

RUSSELL, T. W. F. & CHARLES, M. E. 1959 The effect of the less viscous liquid in the laminar flow of two immiscible liquids. *Can. J. Chem. Engng* **39**, 18.

RUSSELL, T. W. F., HODGSON, G. W. & GOVIER, G. W. 1959 Horizontal pipeline flow of mixtures of oil and water. *Can. J. Chem. Engng* **37**, 9.

SHERTOK, J. T. 1976 Velocity profiles in core–annular flow using a laser-Doppler velocimeter. Ph.D. thesis, Princeton University.

SMITH, M. K. 1989 The axisymmetric long-wave instability of a concentric two-phase pipe flows. *Phys. Fluids* A **1**, 494.

STEIN, M. H. 1978 Concentric annular oil–water flow. Ph.D. thesis, Pursue University.

YU, H. S. & SPARROW, E. M. 1967 Stratified laminar flow in ducts of arbitrary space. *AIChE J.* **13**, 10.